YILDIRIM BEYAZIT UNIVERSITY

GRADUATE SCHOOL OF NATURAL AND APPLIED SCIENCES

MAXIMUM POWER POINT CONTROL OF THE PHOTOVOLTAIC WATER PUMP WITH SEPARATELY EXCITED DC MOTORS

M.Sc. Thesis by

MUSTAFA EMRE ARAS

Department of Computer Engineering

February, 2016

ANKARA

MAXIMUM POWER POINT CONTROL OF PHOTOVOLTAIC WATER PUMP WITH SEPARATELY EXCITED DC MOTORS

A Thesis Submitted to

the Graduate School of Natural and Applied Sciences of Yıldırım Beyazıt University

In Partial Fulfillment of the Requirements for the Degree of Master of Science of Philosophy in Computer Engineering, Department of Computer Engineering

by

Mustafa Emre ARAS

February, 2016

ANKARA

M.Sc. THESIS EXAMINATION RESULT FORM

We have read the thesis entitled **"MAXIMUM POWER CONTROL OF THE PHOTOVOLTAIC WATER PUMP WITH SEPARATELY EXCITED DC MOTORS"** completed by Mustafa Emre ARAS under supervision of **Prof. Dr. Abdullah ÇAVUŞOĞLU** and we certify that in our opinion it is fully adequate, in scope and in quality, as a thesis for the degree of Master of Science.

Prof. Dr. Abdullah Çavuşoğlu

(Supervisor)

Prof. Dr. Fatih Vehbi Çelebi

(Jury Member)

Doç. Dr. Remzi Yıldırım

(Jury Member)

Prof. Dr. Fatih Vehbi Çelebi

(Director)

Graduate School of Natural and Applied Sciences

ETHICAL DECLERATION

I have prepared this dissertation study in accordance with the Rules of Writing Thesis of Yıldırım Beyazıt University of Science and Technology Institute;

- Data I have presented in the thesis, information and documents that I obtained in the framework of academic and ethical rules,
- All information, documentation, assessment and results that I presented in accordance with scientific ethics and morals,
- I have gave references all the works that I were benefited in this dissertation by appropriate reference,
- I would not make any changes in the data that I were used,
- The work presented in this dissertation I would agree that the original,

I state, in the contrary case I declare that I accept the all rights losses that may arise against me.

MAXIMUM POWER POINT CONTROL OF THE PHOTOVOLTAIC WATER PUMP WITH SEPARATELY EXCITED DC MOTORS

ABSTRACT

This paper proposes a new off grid water pumping system design with a new maximum power point tracking method. The photovoltaic water pump is composed of a separately excited DC motor, the centrifugal pump, motor driver and maximum power point tracking unit. In the thesis, each subsystems are explored in detail and then, the proposed frequency controlled MPPT method is defined. Moreover, the drive electronics and control software for the centrifugal pump connected separately excited DC motor is designed. The proposed MPPT method is based on controlling the switching frequency of the DC step down chopper circuit and therefore the loss in energy due to complex DC-DC converters in the other MPPT control units is not observed in the proposed off grid water pump. During the PV water pump tests, at various Solar irradiation levels the voltage, current, power, rpm, flow rate and pressure rate data are recorded and then analyzed. It is concluded that the proposed MPPT method increase the delivered power and therefore it is observed that performance and efficiency of the PV water pump are increased compared to without the MPPT method controlled PV pumps.

Keywords: Photovoltaic pumping system, maximum power point, maximum power point tracking, step down chopper circuit, matching, separately excited DC motor, centrifugal pump.

FOTOVOLTAİK SU POMPASININ DIŞARIDAN UYARTIMLI DC MOTORLAR İLE MAKSİMUM GÜÇ NOKTASI KONTROLÜ

ÖZET

Bu çalışmada yeni bir maksimum güç noktası takip methoduyla beraber yeni bir şebeke bağlantısız fotovoltaik su pompası system tasarımı önerilmektedir. Bu fotovoltaik su pompası; dışardan uyartımlı DC motor, santrifüj pompa, motor sürücüsü ve maksimum güç noktası takipçisi ünitesinden oluşmaktadır. Bu tezde herbir alt sistem detaylı bir biçimde araştırıldı ve sonra önerilen frekans kontrollü MPPT method tanımlandı. Dahası, santrifüj pompaya bağlanan dışarıdan uyartımlı DC motor için sürücü elektroniği ve kontrol yazılımı tasarlandı. Önerilen MPPT methodu azaltan DC kıyıcı devresinin açma kapama frekansının kontrol edilmesine dayalıdır ve bu yüzden diğer MPPT ünitelerinde yer alan karmaşık DC-DC dönüştürücülerinde görülen enerji kayıpları önerilen şebeke bağlantısız fotovoltaik su pompasında görülmez. Fotovoltaik su pompası testleri süresince, çeşitli Solar ışıma değerlerinde voltaj, akım, güç, devir, debi ve basınç değerleri kaydedilerek analiz edildi. Önerilen MPPT methodunun dağıtılan gücün arttırdığını ve bu nedenle fotovoltaik su pompasının MPPT methodu kullanmadan kontrol edilen fotovoltaik pompalara karşılaştırıldığında performansının ve verimliliğinin daha yüksek olduğu gözlemlenmiştir.

Anahtar sözcükler: Fotovoltaik su pompası sistemi, maksimum güç noktası, maksimum güç noktası takipçisi, alçaltıcı DC kıyıcı devresi, yük eşleşmesi, dışarıdan uyartımlı DC motor, santrifüj pompa.

ACKNOWLEDGEMENTS

I would like to acknowledge my tutor and supervisor Prof. Dr. Abdullah Çavuşoğlu, for his support, encouragement and enthusiasm throughout the graduate program and the works related with the thesis. It has been an honor and a pleasure for me to work with him.

I would also like to express my gratitude to Prof. Dr. Fatih Vehbi Çelebi for his feedback, support and guidance.

Finally, I would like to thank my parents, my friends, for their supports and advices through the researches and works.

2016, 1 February Mustafa Emre ARAS

CONTENTS

ABBREVATIONS

Maximum Power Point Tracking	(MPPT)
Maximum Power Point	(MPP)
Photovoltaic	(PV)
Perturb and Observe	(P&O)
Incremental Conductance Technique	(ICT)
Kirchhoff's Voltage Law	(KVL)
Maximum Power Voltage	(Vmpp)
Maximum Power Current	(Impp)
Continuous Conduction Mode	(CCM)
Discontinuous Conduction Mode	(DCM)
Safe Operating Area	(SOA)
Reverse Biased Safe Operating Area	(RBSOA)

LIST OF TABLES

LIST OF FIGURES

CHAPTER 1

INTRODUCTION

The interest in photovoltaic applications are increasingly developing since in remote areas there are lack of power line close to irrigation zones, failures occurs in meeting the rising load that is caused by the frequent electric shortage, environmental degradation is produced by the fossil fuel sourced power plants, cost of the electricity that is generated by the fossil fuel source is high and the generated electric cost of PV plants has been decreased [1]. Photovoltaic water pump applications lessen the minimum level the dependence on diesel, gas or coal based electric generation. The diesel or propane usage in the water pump applications requires high cost and also causes noise and air pollution. In comparison with the Solar water pump, the overall cost, operation and maintenance cost and replacement cost of diesel water pump are 2-4 times higher [2]. Moreover, photovoltaic water pumps have crucial advantages over diesel water pumps in terms of system efficiency, sustainability and payback time. Therefore, various researches about photovoltaic water pumping systems with different topologies have been explored. The topologies are related to the motor type, motor driver and MPPT tracking methods.

In this thesis a new standalone photovoltaic centrifugal water pump with a separately excited DC motor system is presented and the operation of DC motor controller with the proposed MPPT algorithm is evaluated after the tests. Also, power electronics for the motor driver and the MPPT unit is described and analyzed. Safety levels for the switching IGBTs and the diodes are determined by considering switching frequency, power loss and stray inductance and then the snubbers and the gate driver circuit designs are developed.

1.1 Photovoltaic Water Pumps

Photovoltaic water pumps offer various solution for irrigation lands and delivering drinking water since the cost and sustainability is the main criteria for the applications. Also, the photovoltaic water pump installation is easier and could be transferable to other areas. Off grid modular photovoltaic water pumps are a major solution for the agricultural regions in

which limited electric lines along the irrigation source. Moreover, the new additional electric line cost for irrigation lands is higher and therefore payback time for on grid water pumping systems for irrigation is much higher than off grid PV water pumps. In addition, one of the main advantages of the PV water pump is that its maintenance and operating costs are lower.

PV water pumps resemble in many aspects the other water pumping systems and the only difference is that PV water pumps use Solar energy to generate power. The system is composed of photovoltaic panels, the control unit, the motor and the pump [3]. First of all, photovoltaic energy that generated from photovoltaic cells is delivered to the control unit. The control unit is responsible for the power distribution, maximum power point tracking and controlling both the motor and the pump. Secondly, the DC motor uses the photovoltaic energy and converts electric torque to mechanic torque. Then, the mechanical torque is transmitted to pump. The motors used in photovoltaic water pump could be classified as brushless DC motor, AC induction motor and DC motor. Finally, the pump is determined by the irrigation type as surface pump and submersible type. The needed flow rate per minute, pressure and rpm data are the main characteristics for determining the pump.

1.2 The Proposed Photovoltaic DC Motor Coupled Water Pumping System

The proposed photovoltaic water pumping system is designed by considering the load characteristics related with the pump. The PV water pumping system is composed of a surface centrifugal water pump and the electrical characteristic of the DC motor is determined by considering the water pump specifications. Moreover, the operating characteristics of the DC motor is more compatible with photovoltaic water pump applications since there is no need for energy conversion from photovoltaic energy. Therefore, a separately excited DC motor is used for transmitting mechanical torque to centrifugal pump. The separately excited DC motor has advantages of controlling the speed easily by the way changing the field flux rate. As a consequence, the DC motor has been controlled efficiently during start up, constant torque and speed regions without requiring complex drive circuits and algorithms. Furthermore, the MPPT unit in the PV water

pumping system is responsible for both driving the DC motor and enabling the PV array for delivering the maximum power by MPPT methods. For the MPPT tracking a new method that is based on matching load with the PV array by adjusting the operating frequency of the step down DC chopper circuit.

1.2.1 PV Module

Photovoltaic water pump design requires matching between load and photovoltaic. In addition, electrical characteristics of the load must be met by the PV array strings. The PV array combination is designed by considering the electrical characteristics of the DC motor. Therefore, 24 pieces 230W polycrystalline PV modules are used to supply the necessary power for the 5kW DC motor. The photovoltaic array includes 3 parallel strings and each string is composed of 8 serial PV modules. Moreover, the operating voltage and current values of the separately excited DC motor are used to determine maximum power voltage and current of the PV array. In addition, the PV array size is designed by considering various irradiation level and therefore the maximum power point is determined by adjusting the irradiation level close to 1000W/m2. When the irradiation level starts to decrease, the change observed in the maximum power voltage is much higher than maximum power current and therefore a trade-off between reduction in torque rate and revolution could be done. If the DC motor torque is higher than the required centrifugal pump torque then the PV array voltage could be arranged by considering more serial connected PV modules instead of parallel strings. Consequently, the basis of the PV water pump design is matching between electrical characteristics of photovoltaic array and the motor by considering various irradiation levels.

1.2.2 Maximum Power Point Tracker

Directly connected standalone Solar water pumping systems are inefficient due to mismatch of load and operating characteristics of the Solar array. Since armature resistance of the DC motors are too small and force PV array to operate in short circuit region. In addition, after the motor is reached the optimum operating conditions, maximum power point tracking is crucially important for the efficiency of the PV system especially at the time Solar irradiation changes rapidly.

The MPPT unit is consisted of DC motor driver circuit and MPPT circuit. The DC motor driver circuit is an electronic control interface between PV array and DC Motor. It controls the voltage and current rates of the DC motor while performing maximum power point tracking.

The motor driver based on chopper circuits with turn on, turn off and overvoltage snubbers are added inside the MPPT unit for protection. First, IGBT's and gate drivers are the one of the most important parts in driver circuits. IGBT's turn on and turn of times have to be compatible with IGBT driver and snubber circuit designs. Since energy of the both turn on snubber inductor and turn off snubber capacitor has to be discharged for the next period. Moreover, IGBTs that have features of low turn on and turn off are more suitable for both snubber circuits and step down DC chopper circuits. Typical switching frequency of the IGBT gate driver is around 1 kHz - 10 kHz and the rates are higher in comparison with switching frequencies of the inductive motors. Therefore, the snubber loss will be much higher. However, by making suitable snubber design with safety factors, the problem is eliminated. Otherwise, cooling snubber heat sink may become a problem.

The most common methods for maximum power point tracking are incremental conductance and P&O perturb and observation. The algorithms are similar and aim to adjust the operating PV array voltage to optimal maximum power point voltage [4].

This paper presents a new MPPT algorithm that controls the operating frequency of the motor driver for utilizing energy more efficient in changing weather conditions. Frequency controlling method is based on increasing/decreasing the motor resistance by controlling the operating frequency of the step down DC chopper circuits. As a consequence, by controlling motor driver frequency, motor load is controlled and load matching with PV array is accomplished successfully. Overall system efficiency is higher since DC-DC converter is not needed for tracking the maximum power points and power switching devices losses are eliminated. In addition, the reliability of the proposed MPPT unit is higher in comparison with the unit that is composed of complex DC-DC converter units.

1.2.3 DC Motor

In a DC motor, there is a rotating rotor and stationary stator. Armature windings are on the rotor. Armature windings are attached to commutator that rotates with shaft and isolated with each other. Also, the commutator is made of chopper segments. Brushes are made of carbon and let the circuit current flow into commutator and so armature windings. Stationary stator of the DC motor includes wounding circular coils that generate necessary magnetic field for rotor rotation. Field flux of the DC motor is produced when field current applied to circuits [5]. DC motors are classified as permanent magnet, separately excited and self excited DC motors. In addition, the self excited DC motors could be classified as shunt, serial and compound DC motors by the connection type of armature and field circuits.In addition, self-excited DC motors could be classified as series and shunt DC motors. Separately excited, series and shunt motors are the most common the DC motors that are used in PV water pump applications.

First, the electrical characteristic of the series DC motor is more suitable for directly connected PV water pumps. The series DC motor could start to rotate by itself since the voltage level of load-PV intersection point is suitable for the DC motor to start up by itself. After the series DC motor starts to rotate, the voltage across its terminal increases.

Secondly, the shunt DC motor can't start to operate on itself since armature resistance is too small and the load-PV intersection point is close to short circuit point level. In addition, the shunt DC motor needs also necessary magnetic field to rotate armature and without a motor driver circuit magnetic field couldn't be produced. Therefore, a motor driver circuit is needed to start up the motor and enable the load matching with the PV array.

Finally, separately excited DC motors are compatible with PV water pumping application Also, if a driver circuit is used in the PV water pumping system then operation of the DC motor will be easy and efficient. Moreover, the separately excited DC motor has advantages of high efficiency, constant torque, efficient pwm controlled chopper drive system, and low starting current. As a consequence, the DC motor working characteristics are compatible with PV water pump applications and the system efficiency is higher without the DC-AC conversion.

1.2.4 The Centrifugal Pump

The centrifugal pump is one of the common water pump type used in irrigation application. Since the structure of the pump is simple, robust and efficient for the pumping applications. The centrifugal pump types differ by the application area and therefore it could be categorized as surface and submersible centrifugal pump. In the proposed PV water pumping system, a surface pump is used and the connection between the centrifugal pump and motor is performed by using a coupling on the motor shaft. As a consequence, the mechanical torque is transmitted to the centrifugal pump. Moreover, when the pump starts to operate a fluid pressure is created from the pump inlet to its outlet. The pressure difference leads the water to flow inlet to outlet direction. Also, if the speed of the shaft increases, the flow rate and pressure of the water increase in a rate determined by the equations of the centrifugal pump.

1.3 Scope of the Thesis

The proposed photovoltaic water pumping system that is consist of PV array and MPPT unit connected separately excited DC motor is evaluated in this thesis. In addition, the operating characteristics of the DC motor is analyzed by using complex drive algorithms and a new proposed MPPT method.

Load matching with PV array is the main purpose of standalone PV water pumps. Efficiency of directly connected Solar DC water pumps and their performance analysis are evaluated and analyzed in the experiments [6-9]. Moreover, common MPPT methods perturb and observations (P&O) and incremental conductance technique (ICT) used in DC-DC converters are evaluated and analyzed in researches [10-13].

Although, many experiments about common MPPT methods such as ICT, constant voltage and P&O methods are presented in literature, frequency and switch mode DC-DC converter based MPPT algorithms for the PV water pumping systems are not evaluated deeply.

Frequency controlled DC step down chopper circuit and switch mode MPPT circuits for separately excited DC motor connected PV water pumps are examined. Also, snubber circuits for the motor controller and soft starter circuits for motor controller are presented.

CHAPTER 2

PHOTOVOLTAIC MODULES

2.1 Introduction

In this chapter electrical characteristics of PV cells are explained and datasheet of a PV module is analyzed by considering temperature coefficients and various Solar irradiance levels. To begin with, the PV cell model is defined and formulas for operating characteristics of the PV Cell is derived. Also, operating characteristic of the PV cell is shown in I-V curve and specific points are described: Open Circuit Voltage (Voc), Short Circuit Current (Isc), Maximum Power Point (Vmpp), Maximum Power Voltage (Vmpp) and Maximum Power Current (Impp). Moreover, the power curve is shown and its relation with the I-V curve is evaluated. Finally, the way how to associate PV modules for reaching determined voltage and current rates are explored.

2.2 Electrical Characteristics of the PV Cell

Semiconductor materials in Solar cell enable to be electrically conductive when exposed to heat or light. Doping technique is applied for creating positive charge carriers (p-type) or negative charge carriers (n-type). After the doping application a p-n junction is formed by the connection of the two layers. Then, the light causes to releasing of charge carriers and then internal electric field separates the charge carriers. By the photons crash effect free electrons within the electric field boundary are pulled p-side to n-side [14]. As a consequence, when an external circuit is connected, then an electric current flows from p-side to n-side.

PV cell equivalent electric circuit model includes a photocurrent, a diode, a parallel resistor for showing leakage current, and a series resistor defines internal resistor for current flow. The PV cell circuit model is shown in Figure 2.1.

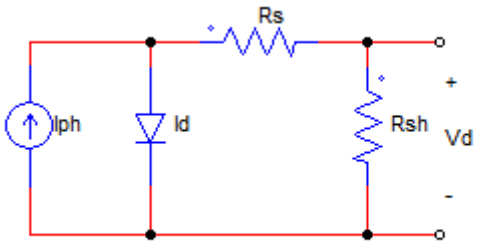

Figure 2.1 Equivalent circuit of PV Cell

PV cell equivalent circuit equations are derived by using the *Kirchhoff's* Voltage Law (KVL) in the loops in Fig.2. In the circuit R_s value is close to zero and since R_{sh} value is very large, it closes to infinity [15]. By taking considerations the approaches, following equations show the formulas for the equivalent circuit of a PV cell:

$$I = I_{ph} - I_d \tag{2.1}$$

In the equations: I is the output current, I_d represents the temperature dependent diode current and I_{ph} is the light generated current.

The current through the diode is defined by the following equations:

$$I_d = I_o\left(e^{\frac{qV_d}{nkT}} - 1\right) \tag{2.2}$$

Where:

I_o: the diode leakage current density

V_d: Voltage of the Solar cell

T: the temperature of the PV cell

q: defines the electron charge (q=1.602e-19 C)

k: Boltzmann constant (k=1.38e-23)

n : Empirical constant

Leakage current Io is defined by the following equations:

$$I_o = I_{sc}\left(\frac{T}{T_{ref}}\right)^3 e^{\frac{qE_g}{nk}\left(\frac{1}{T_{ref}}-\frac{1}{T}\right)} \quad \textbf{(2.3)}$$

Where:

I_{sc}: Short circuit current of the PV cell

E_g: Band gap energy of the semiconductor

T_{ref} : Reference temperature

$$I_{ph} = \frac{\emptyset}{\emptyset_{ref}}\left(I_{scr} + \alpha_{isc}(T - T_{ref})\right) \quad \textbf{(2.4)}$$

$\emptyset$: Solar irradiation

$\emptyset_{ref}$: Reference Solar irradiation

α_{isc}: Short circuit current temperature coefficient of the PV cell,

I_{scr}: Short circuit current of the PV cell at a reference temperature

2.3 PV Module Output Characteristics: P-V and I-V Curves

PV cells could operate on broad range between minimum and maximum levels of its current and voltage rates. The operating point is determined by the intersection point of load and PV source on the I-V graphic of the PV module as shown in Figure 2.2.

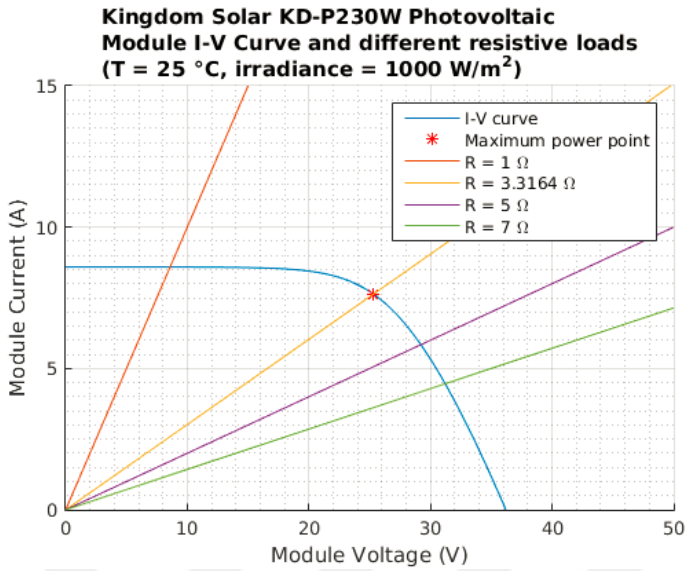

Figure 2.2 I-V curves of KDM 230P PV module and various load connections

Moreover, the specific operating points on the PV module is defined and shown in Figure 2.3. In the figure, open circuit voltage Voc defines the point when the load is opened and therefore the power output is zero. Vmpp and Impp points describe the operating point when the delivered power is maximum. Isc is the short circuit point in which the PV module is short circuited and therefore the output power is zero at this point. Furthermore, P-V characteristics of the PV panel is shown in Figure 2.4.

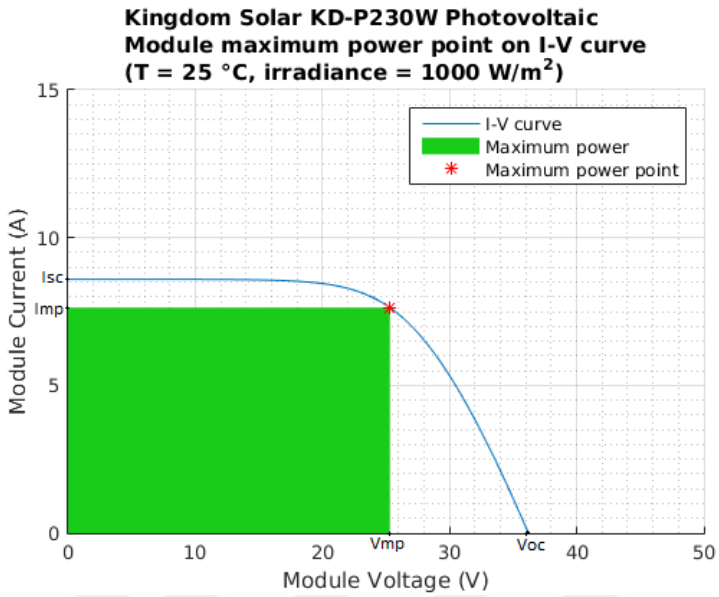

Figure 2.3 I-V curves of KDM 230P PV module and specific operating points

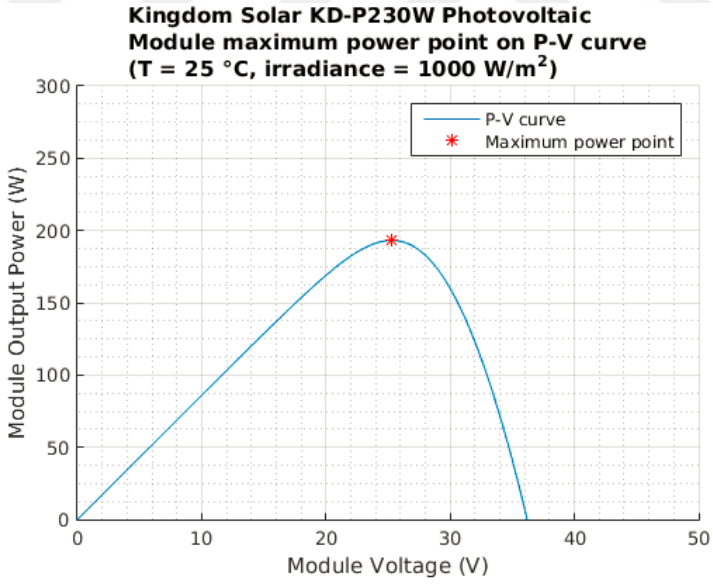

Figure 2.4 P-V characteristics of the KDM 230P PV module

The P-V curve shows that increasing voltage enable power rate to rise until the Vmpp point is reached. Then, the P-V curve decreases and at Voc point the power becomes zero. When the PV cells are operating at maximum power points, the internal resistance of the PV cells match with load resistance and thus the maximum power transfer occurs.

Performance of the PV cells is affected by the irradiance and temperature values. Efficiency of the PV cells increase directly with rising insolation. In addition, a decrease in insolation level or partial shadowing effect cause the PV cell to operate in lower performance. As seen in Figure 2.5, the Isc increases linearly with the increase in Solar irradiation. However, the open circuit voltage Voc increase in a smaller rate.

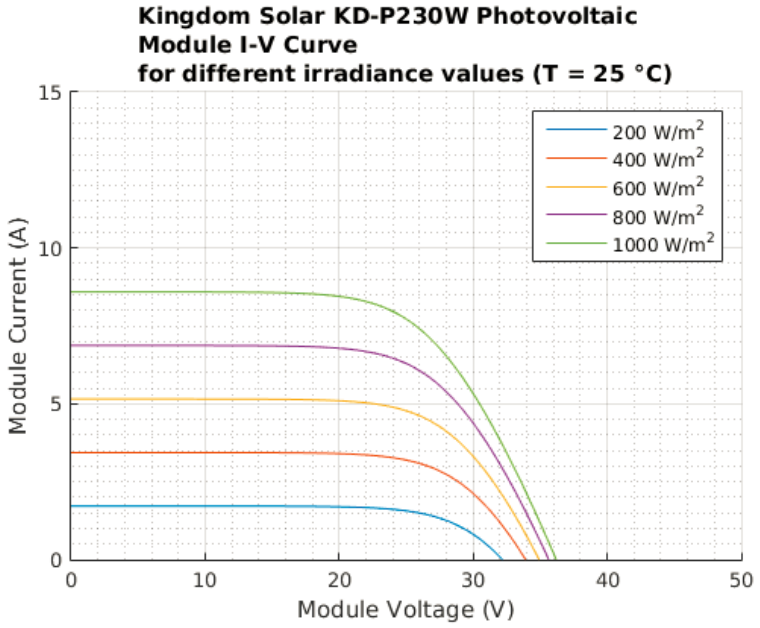

Figure 2.5 PV module I-V graphic at various Solar irradiation

Moreover, the P-V relation with Solar irradiation is shown in Figure 2.6 and by the way increasing Solar irradiance the change in maximum power point is much less. The relation between the light generated current and Solar irradiation is given in equation (2.4).

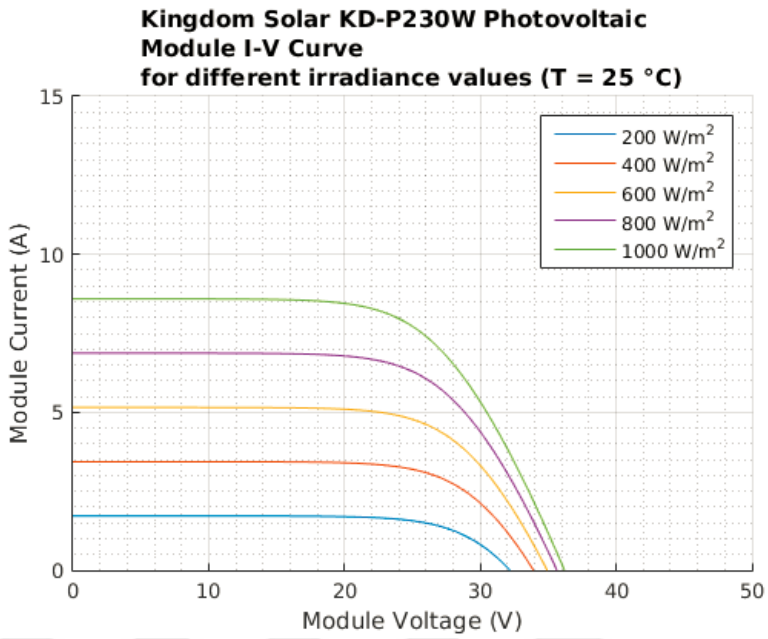

Figure 2.6 PV module P-V graphic at various Solar irradiation

Furthermore, temperature effects on the I-V characteristic of the PV module is given in Figure 2.7. While the temperature value increasing, the short circuit value increases and open circuit value decreases. In addition, the power rate decreases with the increasing current effect [16]. The relation between the light generated current and temperature is also given in equation (2.3**).**

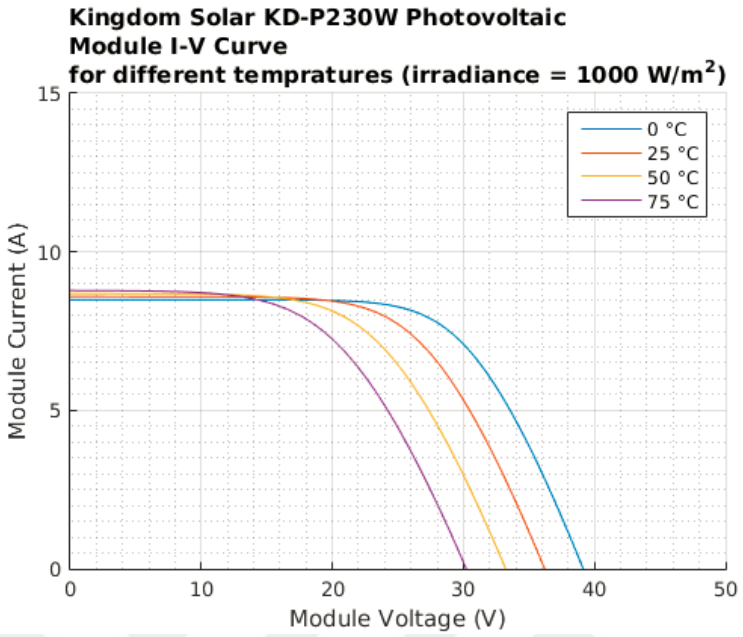

Figure 2.7 PV module I-V graphic at various temperature rates

2.4 PV Module and Array Design

Since a PV module voltage and current values are limited, many PV modules could be combined serial and parallel to reach defined PV array voltage and current size. PV modules in an array behave like batteries since when they are connected in parallel their voltage stays same, however, the output current rate is the sum of two panels. Moreover, when PV modules are connected in serial, the output voltage becomes the sum of two panel voltages. However, the output current rate stays same. As a consequence, PV array combination is performed by designing the row and column numbers of the strings and thus PV source matches with the electrical characteristics of the load.

CHAPTER 3

DC MOTORS AND CENTRIFUGAL WATER PUMPS

3.1 Introduction

In this chapter the motor and centrifugal pump used in PV water pumping systems are described and evaluated. String size and voltage of the PV array are calculated by using electrical and mechanical data of the motor and pump. Since, the requirements for the photovoltaic water pump application such as flow rates per minute and water pressure are the main parameters for choosing the pump. Then the required rpm and torque data for the pump are used for determining the electrical and mechanical characteristics of the motor. First, separately excited DC motors are described and then electrical and mechanical characteristics of the motors are explored. Also, the electrical and mechanical equations are derived and explained. Secondly, operating characteristic of the separately excited DC motor is explored. Therefore, starting, no load, behavior when loaded and steady state operation topics are described. Finally, the centrifugal water pump used in the photovoltaic application is evaluated by deriving its mechanical equations.

3.2 Separately Excited DC Motors

DC motors use direct current source to convert electrical energy into mechanical energy. The main structure of the DC motor consists of the stator and the rotor. The stator carry field windings or magnets to produce magnetic flux. The rotor includes armature winding and the continuous winding is connected to commutator segments. Stationary terminals of the armature winding provides the DC voltage and current to commutator segments by using the at least one pair of stationary carbon brushes [17] DC motors are categorized by the connection type of field winding to armature winding as separately excited, self excited and permanent magnet DC motor. Self excited and permanent magnet DC motor and their electrical and mechanical characteristics are evaluated in the literature [18-21].

In the proposed photovoltaic water pumping system a separately excited DC motor is used for converting the photovoltaic energy into mechanical energy. The separately excited DC motors is composed of armature and field circuit across a DC supply. Also, field circuit could be used for controlling speed and torque. Field current is directly proportional to field flux $\emptyset_f$ with field constant parameter. The equation is represented by the following formula:

$$\emptyset_f = k_f I_f \quad \textbf{(3.1)}$$

Where:

k_f is a field constant of proportionality. Total flux $\emptyset_f$ interacts the armature current i_a and then electromagnetic torque is generated.

$$T_{em} = k_t \emptyset_f i_a \quad \textbf{(3.2)}$$

Where:

T_{em} is the electromagnetic torque and k_t is the torque constant of the motor. Back emf produced in armature circuit by the rotation of the armature in the effect of field flux $\emptyset_f$ can be written in the form:

$$e_a = k_e \emptyset_f \omega_m \quad \textbf{(3.3)}$$

Where:

k_e is the voltage constant of the motor and ω_m is the speed. Equivalent circuit of the DC motor is shown in Figure 3.1.

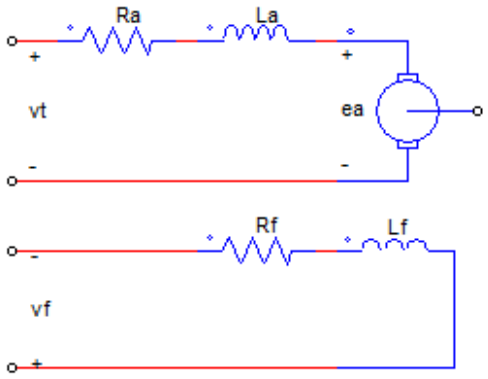

Figure 3.1 Equivalent circuit of the separately excited DC motor

In the circuit the following dynamic and steady state equations of the DC motor are derived by applying the Kirchhoff Voltage Law:

Dynamic Equations:

$$v_t = R_a i_a + L_a \frac{di_a}{dt} + e_a \quad \textbf{(3.4)}$$

$$v_f = R_f i_f + L_f \frac{di_f}{dt} \quad \textbf{(3.5)}$$

$$e_a = K i_f \omega_m \quad \textbf{(3.6)}$$

$$T_{em} = J \frac{d\omega}{dt} + D\omega_m + T_L \quad \textbf{(3.7)}$$

Steady State Equation:

$$V_t = R_a I_a + E_a \quad \textbf{(3.8)}$$

$$V_f = R_f I_f \quad \textbf{(3.9)}$$

$$E_a = K I_f \omega_m \quad \textbf{(3.10)}$$

$$T_{em} = J\omega_m + T_L \quad \textbf{(3.11)}$$

Where:

R: Resistance

V_t: Voltage source

I: Current

L: Inductance

E: Back emf

J=Inertial

D: Damping coefficients

T_L: Load torque

The subscripts a and f represent armature and field circuits related coefficients. The inductive voltage is correspondent to rate of changing current and however, in steady state it becomes zero [22-23]. By using equations **(3.2)**, **(3.5)** and **(3.9)**, ω_m is derived as a fuction of T_{em} for a given V_t and shown in the following equation.

$$\omega_m = \frac{1}{k_e \emptyset_f}\left(V_t - \frac{R_a}{k_t \emptyset_f} T_{em}\right) \quad \textbf{(3.12)}$$

3.2.1 Steady State Operation

The derived steady state speed ω_m for the separately excited DC motor is given by the equation **(3.12)**. The torque and speed control of the motor could be done by controlling the armature voltage and field flux. First, the motor operates with constant torque for the speed less than rated speed level. By the way constant flux the motor electrical and mechanical equations are given below:

$$T_{em} = k_t I_a \quad \textbf{(3.13)}$$

$$E_a = k_E \omega_m \quad \textbf{(3.14)}$$

The terminal voltage increase linearly up to its rated value and since the armature resistance is too small, the slope starts very close to zero. Also the speed has a direct slope that starts approximately from zero. The steady state operation in the torque-speed plane for the separately excited DC motor is given in Figure 3.1. When the armature voltage reaches its full voltage with the full field flux condition, the corresponding speed value is defined as base speed. The region is referred as constant torque region since the motor can operate at full rated torque and the speed reaches zero to its base value. Also, the produced mechanical power is calculated by multiplying torque and speed values and therefore the power along ab is directly proportional with the speed value. At point b, the full power is produced. In addition, the voltage and current rates are at their full values.

The speed could be increased above base speed value by decreasing the field flux. The field flux reduction is defined as field weakening and done by decreasing field current. Also, V_t is stayed constant and I_a is forced to stay its rated value for continuity requirement. The region is also named as constant power region since maximum power stayed constant. However, the torque decreases with the reduced flux and then the speed increases correspond to the decrease in the torque level. Field weakening region may applicable for the operation that does not require full torque at high speeds [24]

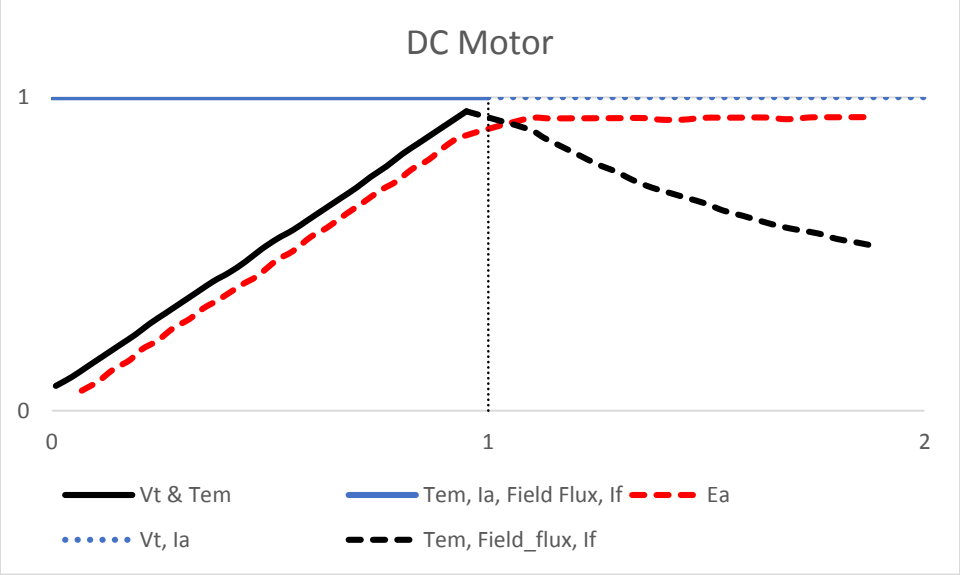

Figure 3.2 Steady state operation in the torque-speed plane

3.2.2 Dynamic Operation

Dynamic operation takes place when the sudden current change occurs in the motor. In addition, the armature inductance is the main source of the effects of the dynamic change since the sudden changes about the current level enable the inductor to store energy. Moreover, rotary kinetic energy is stored in the inertia by the way sudden change in speed. The transient dynamic of the DC motor is governed by electromechanical and electrical time constants.

First of all, the sudden speed change in the motor is determined by the electromechanical time constant and therefore the speed reaches a new level by the way a change occurs in the armature voltage or load torque. The applied voltage and load torque are main parameters for changing steady state operation of the motor. If the armature inductance is ignored then the transient operation could be represented by first order exponential responses in the speed and current by the following equation.

$$i = \left(\frac{V_2 - V_1}{R}\right) e^{-t/\tau} \qquad \textbf{(3.15)}$$

Moreover, if the armature voltage is increased from V_1 to V_2 in a frictionless and unloaded motor, then a sudden current increase is observed in Figure 3.3. In addition, the increased current rises the torque since back emf is lower than the applied voltage. Then, the speed and back emf increases by the sudden change in the current and the current starts to fall zero.

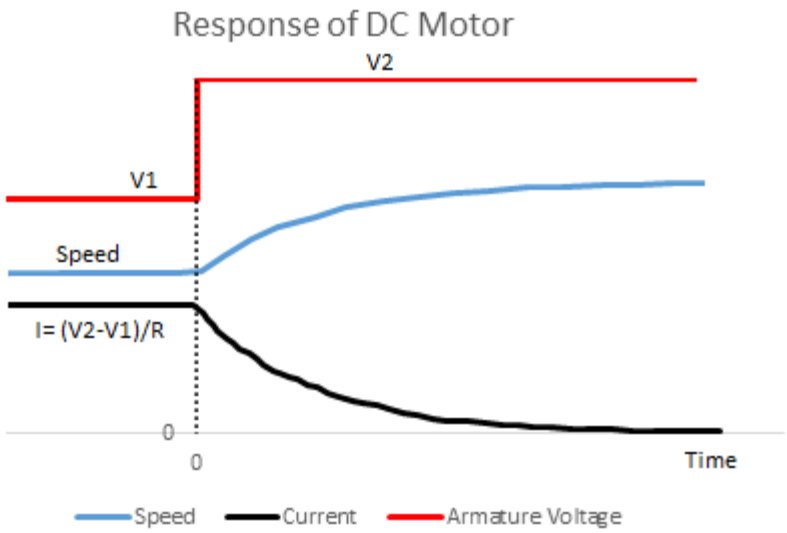

Figure 3.3 Step increase characteristics of the DC motor

The time constant is derived in terms of the motor parameters by the following formula.

$$\tau = \frac{RJ}{k^2} \qquad \textbf{(3.16)}$$

Where:

R: Armature resistance

J: Total rotary inertia

k: Motor constant

The equations shows that electromechanical time constant is related with electrical parameters R and k and mechanical parameters J. The increment rate of the electrical parameters R and k are not effective as the mechanical parameter J.

Secondly the electrical time constant defines the required time for steady state after the sudden change that occurs in armature current immediately following a change in armature voltage [25]. The armature time constant is given by the following formula:

$$\tau_a = \frac{L}{R} \qquad \textbf{(3.17)}$$

Consequently, electromechanical time constant are more prolonged than the electrical time constant.

3.3 Centrifugal Pump

Photovoltaic water pump applications are consisted of the motor connected pumps. Torque and speed characteristics of the motor should be compatible with the pump rates. In addition, the application defines the load characteristics and therefore a suitable pump should be selected in terms of starting, steady state and dynamic characteristics. The common pump types that are used in photovoltaic applications are volumetric and centrifugal pumps. In literature, the working efficiency of the centrifugal and volumetric pumps within photovoltaic water pump applications are analyzed and it is concluded that centrifugal water pumps could operates longer for low level insolation. In addition, load characteristics of the centrifugal pumps are more efficient for matching the maximum power points of the PV source [26]. Therefore, the proposed PV water pump is consisted of the DC motor connected a centrifugal pump. The mechanical load torque for the DC motor connected centrifugal pump is related to angular frequency and expressed by the following formula:

$$t_L = A + B\omega^2 \quad \textbf{(3.18)}$$

Where the constants A and B are specific centrifugal pump characteristics. Also, the characteristic curve of the centrifugal pump about the pumping head "*H*" is shown by the following equation:

$$H = A_1S^2 + B_1SQ + C_1Q^2 \quad \textbf{(3.19)}$$

Where S represents the angular speed in rpm and then A1, B1 and C1 are defined as coefficients for the centrifugal pumps.

CHAPTER 4

MAXIMUM POWER TRACKING UNIT

4.1 Introduction

Maximum power point tracking unit provides load matching with the maximum power locus of the PV source and by the way photovoltaic power remains at its maximum level for varying environmental parameters such as irradiation and temperature. In the literature many MPPT methods are introduced and compared with each other by considering complexity, cost, convergence speed, required sensors, implementation hardware and the effects of environmental parameters [27].

In this chapter the common and efficient MPPT methods are described. In addition, the comparison results for tracking efficiency among the MPPT methods are given and evaluated. Moreover, the basic DC-DC converter circuits used in MPPT units are presented and the control methods for the switching devices of the DC-DC converter are explored.

4.2 Maximum Power Point Tracking Methods

Photovoltaics could operate on many points along the its I-V curve according to load characteristic, however, the MPPT enable to deliver maximum power to load by adjusting PV output voltage and current values. In addition to this, the MPPT unit includes a DC-DC converter and switching duty cycle of the converter is controlled by the MPPT method.

MPPT methods have been developed for tracking MPPs to deliver maximum PV power to load. Shading effect, temperature, irradiation and load characteristics are basic parameters that affecting PV module working characteristics. Some MPPT methods are inefficient for tracking MPPs due to the parameters. Moreover, the maximum PV energy is delivered to load by controlling the DC-DC converter since the load impedance that is seen by PV source is adjusted for load matching with the maximum power points to transfer the maximum power. The location of mpp is detected by either through calculations or search algorithms [28]. Below, the common incremental conductance (ICT) and perturb

and observe (PAO) algorithms are explained and their advantages and disadvantages are presented.

4.2.1 Incremental Conductance Technique

Incremental Conductance algorithm declares that derivative of power with respect to PV voltage is zero at MPP, positive for left side of the MPP and negative for the right side of the MPP. In addition, ICT algorithm determines the direction of movement along the P-V curve by taking into consideration the changes occur in PV voltage and current values. The following equations are derived for determining the perturbation direction.

When the operating point is on MPP:

$$\frac{dP}{dV} = 0 \quad \textbf{(4.1)}$$

When the operating point is on left side of MPP:

$$\frac{dP}{dV} > 0 \quad \textbf{(4.2)}$$

When the operating point is on the right side of MPP:

$$\frac{dP}{dV} < 0 \quad \textbf{(4.3)}$$

Then $\frac{dP}{dV}$ is written in terms of voltage and current. Since the equations are derived in terms of voltage and current, the MPPT tracking algorithm is rearranged and determined by two parameters. Therefore, the results become more accurate [29-35]. The equations are given below.

$$\frac{dP}{dV} = \frac{d(VxI)}{dV} = I\frac{dV}{dV} + V\frac{dI}{dV} = I + V\frac{dI}{dV} \quad \textbf{(4.4)}$$

When the operating point is on MPP:

$$I + V\frac{dI}{dV} = 0 \quad \textbf{(4.5)}$$

$$\frac{dI}{dV} = -\frac{I}{V} \quad \textbf{(4.6)}$$

When the operating point is on the left side of MPP:

$$I + V\frac{dI}{dV} > 0 \quad \textbf{(4.7)}$$

$$\frac{dI}{dV} > -\frac{I}{V} \quad \textbf{(4.8)}$$

When the operating point is on the right side of MPP:

$$I + V\frac{dI}{dV} < 0 \quad \textbf{(4.9)}$$

$$\frac{dI}{dV} < -\frac{I}{V} \quad \textbf{(4.10)}$$

Environmental conditions affects the working characteristic of the photovoltaic. Irradiation and temperature are the main parameters that change MPP and P-V diagram of the PV array. ICT algorithm has advantages over the common MPPT techniques, since the dP/dV can give accurate direction for moving forward to MPP. The flow chart of the ICT is given in Figure 4.1. Moreover, since the tracking direction is right, fast tracking is observed. Also, oscillations around MPP are shorter.

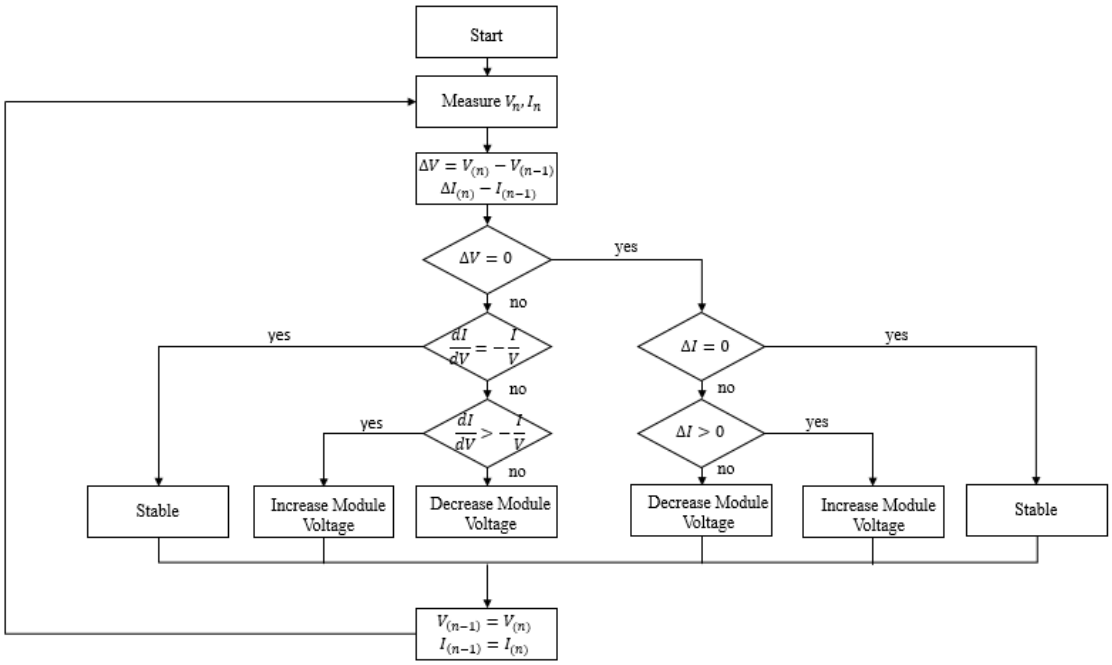

Figure 4.1 Flow chart of the ICT method

4.2.2 Perturb and Observation Method

The Perturb and Observation is the one of common MPP tracking methods. The P&O algorithm tracks the maximum power points by perturbing the duty ratio of the converter in order to change the current and voltage of the PV array and then by comparing PV power with respect to previous PV output voltage and current rates [36-38]. The perturbation direction is determined by changing the voltage and observe the power difference. When $dP/dV > 0$ the perturbation direction is right to reach MPP. The perturbation continues until the MPP point is reached. Moreover, if the algorithm observes the condition $dP/dV < 0$, that means the perturbation is in the wrong direction. Therefore, the perturbation is reversed by the MPP method. The perturbation continues until the power rate starts to decrease. When operating point is reached to MPP level then the perturbation oscillates around the MPP. The PAO method and is operation paths is as shown in Figure 4.2.

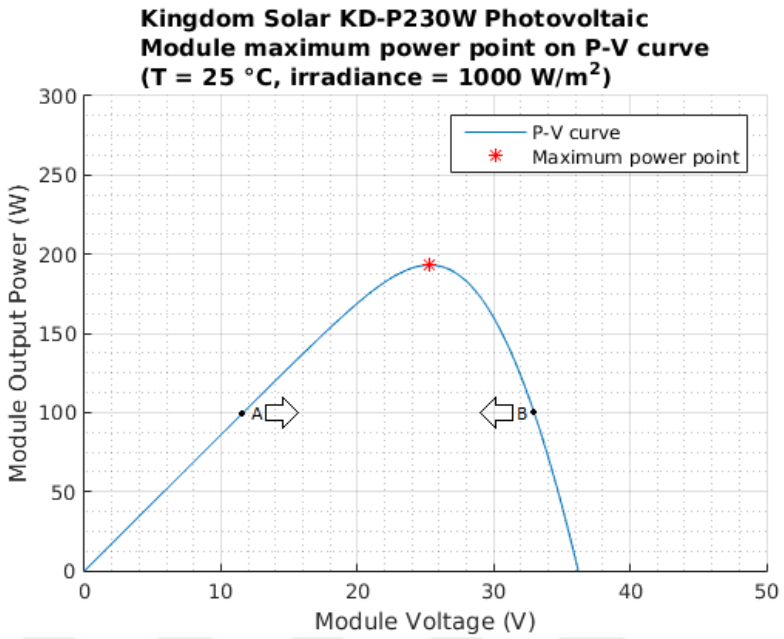

Figure 4.2 The PAO method and its operating paths

The flow chart of perturb and observation method is shown in Figure 4.3. If the effects of environmental parameters are eliminated, the operation of the P&O method is easy and efficient. Especially, the shading effect and the change observed in Solar irradiance are the main environmental parameters that change the MPP. The main disadvantage of the P&O is that an increase in irradiance will lead the perturbation direction to wrong path. Although the shading effect and changing irradiance are a crucial constraint for the MPPT method various algorithms that manage the step size of the perturbation could be used to track the MPP efficiently [38-43].

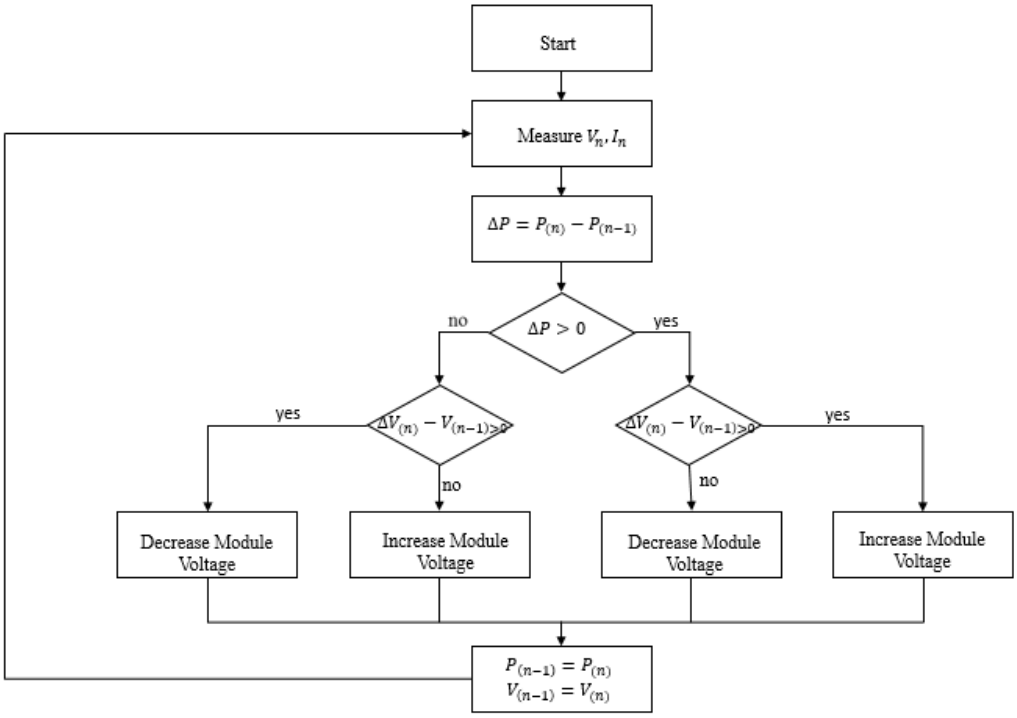

Figure 4.3 Flowchart of the PAO method

4.3 DC-DC Converters

The DC-DC converters are main component of MPPT units. PV-load characteristic is adjusted by switching on /off transistor in DC-DC converters according to MPPT algorithms. MPPT software uses the data come from current, voltage and temperature sensors to control DC-DC converters for MPP tracking. Common MPPT units include the following DC-DC converters:

1. Step down (Buck) Converter

2. Step up (Boost) Converter

3. Step-down /Step up (Buck-Boost) Converter

4. Cúk Converter

The DC-DC converters convert the operating PV voltage into the Vmpp of PV by increasing or decreasing duty cycle of switches in DC-DC converters according to MPPT algorithms. Step down and Step up converters are inefficient if they are used alone. Since they could not both increase and decrease PV operating voltage. Moreover, buck-boost and Cúk converters capable of both increasing and decreasing output voltage. However, their efficiencies are lower than both step up and step down converters. Therefore, some DC-DC converters use both Step up and Step down converters to increase and decrease output voltage. In the MPPT unit, the DC-DC converter circuit includes a switch to open/close the Step up and Step down converters.

4.3.1 Step down (Buck) Converter

Step down converter regulates the average output voltage V_o lower than input voltage Vs. The circuit is shown below in Figure 4.4 and a pwm controlled switch, diode, filter capacitor, filter inductor, and load resistance. According to switch position the average output value is derived. By controlling duty cycle ratio output voltages V_o can be adjusted related to input voltage V_s and the equations are expressed as

$$(V_s - V_o)DT = -V_o(1 - D)T \quad \textbf{(4.11)}$$

$$V_o = DV_s \quad \textbf{(4.12)}$$

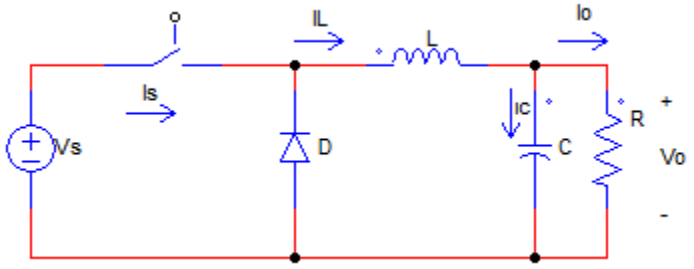

Figure 4.4 Step Down converter

Step down converter has two operation modes according to switching frequency and load value: continuous conduction mode (CCM) and discontinuous conduction mode (DCM). First of all, f average inductor current is always continuous due to high value of load or

high frequency switching, then the mode is CCM and the inductor energy is enough for the feeding the load continuously. However, if the inductor energy is not enough for cycling due to low frequency and high load, DC-DC converter operates in DCM. Then the boundary between CCM and DCM modes are defined according to inductor value and the equation is given below [44-45].

$$L_b = \frac{(1-D)R}{2f} \quad \textbf{(4.13)}$$

Secondly, another important parameter to design Buck converter is filter capacitor value since Capacitor values greater than C_{min} prevents small ripple voltage V_r on DC output voltage V_o. It is calculated by the following equation.

$$C_{min} = \frac{(1-D)V_o}{8V_r Lf^2} \quad \textbf{(4.14)}$$

Finally, to design a buck converter switching frequency, passive components value L and C, and load value is R is needed. By calculating L_b and C_{min} values continuous and ripple voltage free lower output voltage can be provided.

4.3.2 Step up (Boost) Converter

Boost Converter has a function of increasing input voltage and delivering higher output voltage in contrast to input voltage. Figure 4.5 shows a Step up (boost) converter and its operating modes according to switch position.

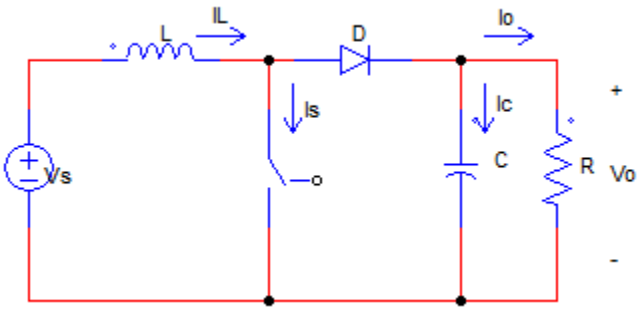

Figure 4.5 Step Up converter

As shown in Figure 4.5 the Step Up converter includes a boost inductor, switch, diode, filter capacitor and load resistance. When the switch is turned on, the energy is supplied to inductor and the diode is off at the time. Then the switch is turned off and both input source and inductor energy is directed into RC circuit. The boost converter circuit equations according to switch position is derived below [46].

$$V_s DT = (V_o - V_s)(1 - D)T \quad \textbf{(4.15)}$$

$$\frac{V_o}{V_s} = \frac{1}{1-D} \quad \textbf{(4.16)}$$

Boost Converter has two operating modes: CCM and DCM. The boundary between CCM and DCM is calculated by using the following formula.

$$L_b = \frac{(1-D)^2 DR}{2f} \quad \textbf{(4.17)}$$

Boost inductor value greater than Lb, enable the converter to operate in CCM. Moreover, to eliminate voltage ripple over load the filter capacitor value must be greater than C_{min} that given below.

$$C_{min} = \frac{DV_o}{V_r RF} \quad \textbf{(4.18)}$$

Finally, to design a boost converter switching frequency, passive components value L and C, and load value is R is needed. By calculating L_b and C_{min} values continuous and ripple voltage free higher output voltage can be provided.

4.3.3 Buck Boost Converter

Buck-Boost Converter could both increase and decrease output voltage in contrast to input voltage. However, the output voltage has a negative polarity. Figure 4.6 shows a buck boost converter and its operating modes according to switch position.

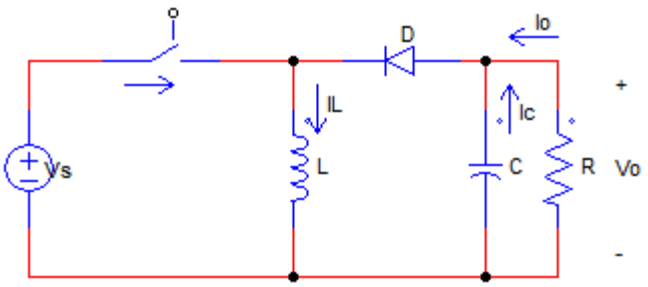

Figure 4.6 Buck Boost Converter

As shown in Figure 4.6 the buck boost converter includes a boost inductor, switch, diode, filter capacitor and load resistance. When the switch is turned on, the inductor current increase and the diode is in off state. Then the switch is turned off and input source connection is opened and just inductor energy is transferred to load. Therefore, buck-boost converter is a combination of both buck and boost converters since has a capability of both increasing and decreasing the output voltage [47-49]. The boost converter circuit equations according to switch position is derived below.

$$V_s DT = -V_o(1 - D)T \quad \textbf{(4.19)}$$

$$\frac{V_o}{V_S} = -\frac{D}{1-D} \quad \textbf{(4.20)}$$

Buck-boost converter has two operating modes: CCM and DCM. The boundary between CCM and DCM is determined by inductor value and calculated by using the following formula.

$$L_b = \frac{(1-D)^2 R}{2f} \quad \textbf{(4.21)}$$

Boost inductor value greater than L_b, enable the converter to operate in CCM. Moreover, to eliminate voltage ripple over load the filter capacitor value must be greater than C_{min} that given below.

$$C_{min} = \frac{DV_o}{V_r RF} \quad \textbf{(4.22)}$$

Finally, buck boost converter output voltage V_o has negative polarity with respect to input voltage. Moreover, if the duty cycle D is equal to 0.5 then, magnitudes of output voltage V_o and input voltage V_{in} are equivalent. However, 50% of input source is not provided during the switch on/off period. Therefore, buck boost converters are less efficient.

4.3.4 Cúk Converter

Cúk converter could both increase and decrease output voltage in contrast to input voltage. However, the output voltage has a negative polarity. The Cúk converter and its operating modes according to switch position are shown in Figure 4.7.

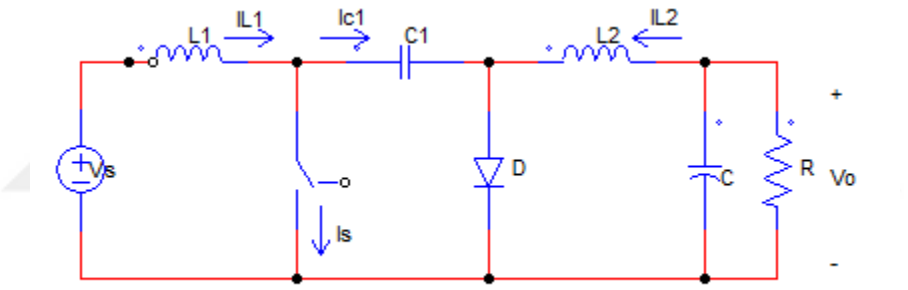

Figure 4.7 Cúk Converter

The converter includes an input inductor, switch, energy diode, energy store and transfer capacitor, filter inductor, filter capacitor and load resistance. When the switch is turned on, the inductor L_1 current increases and the diode is in off state. Capacitor C_1 is discharged through the output and filter inductor L_2. Then the switch is turned off and the energy storage capacitor is charged by both inductor L_1 and input source. The Cúk converter circuit equations according to switch position is derived below.

$$I_{L2} DT = I_{L1}(1 - D)T \quad \textbf{(4.23)}$$

$$\frac{V_o}{V_S} = -\frac{D}{1-D} \quad \textbf{(4.24)}$$

Cúk converter has two operating modes: CCM and DCM. The boundary between CCM and DCM is determined by inductor value and calculated by using the following formula [50].

$$L_{b1} = \frac{(1-D)R}{2Df} \quad \textbf{(4.25)}$$

$$L_{b2} = \frac{(1-D)R}{2Df} \quad \textbf{(4.26)}$$

Both inductor values greater than L_{b1} and L_{b2} enable the converter to operate in CCM. Moreover, to eliminate voltage ripple over load the filter capacitor value must be greater than C_{min} that given below.

$$C_{min} = \frac{(1-D)V_o}{8V_r L_2 f^2} \quad \textbf{(4.27)}$$

Finally, the Cúk converter output voltage V_o has a negative polarity with respect to input voltage. Moreover, if the duty cycle D is equal to 0.5 then, magnitudes of output voltage V_o and input voltage V_{in} are equivalent. The advantages of Cúk converter over buck boost converter is that continuous current flows both input output of the converter.

CHAPTER 5

THE PROPOSED PHOTOVOLTAIC WATER PUMP

5.1 Introduction

The electrical and mechanical characteristics of the proposed PV water pumping system are designed and analyzed in this chapter. The PV water pumping system is consisted of the separately excited DC motor that connected to PV array with the MPPT unit. First, the proposed MPPT method: frequency controlled load algorithm is described and analyzed. The advantages of the proposed MPPT methods are presented. Secondly, control methods for the MPPT circuit and PV array connected separately excited DC motor are described. Therefore, the electrical and mechanical characteristics of the DC motor are presented. Moreover, row and column designs of the PV array are performed by considering the motor electrical characteristics. Then, the step down chopper circuit control method that drives the DC motor connected PV water pump and tracks the MPPs by using the proposed algorithm is analyzed in detail. Finally, power electronics for the MPPT circuit including safety designs are designed and evaluated.

5.2 Proposed MPPT Method: Frequency Controlled Load MPPT Methods

Directly connected standalone PV water pumping systems are inefficient due to mismatch of load and Solar array operating characteristics since armature resistance of the separately excited DC motors are too small and that condition forces PV array to operate in short circuit region. Therefore, the required conditions for the DC motor to start up could not met for the PV source. This paper presents a new MPPT algorithm based on controlling the operating frequency of the DC motor for utilizing the PV energy at optimum level.

First, the motor load is controlled and matching with PV array is accomplished by controlling the operating frequency of the step down chopper circuit that drives the DC motor. The tracking algorithm for the proposed MPPT method is similar to P&O method.

The flow chart of the method is given in Figure 5.1. The motor load rate increases and the operating point that is the intersection point of the load and PV I-V diagram is leaded from left to right by increasing the operating frequency of the DC motor. In addition, the operating points move to left side on the PV I-V graph by decreasing the operating frequency of the DC motor. The MPP is determined by calculating the PV power using the data comes from voltage and current sensors.

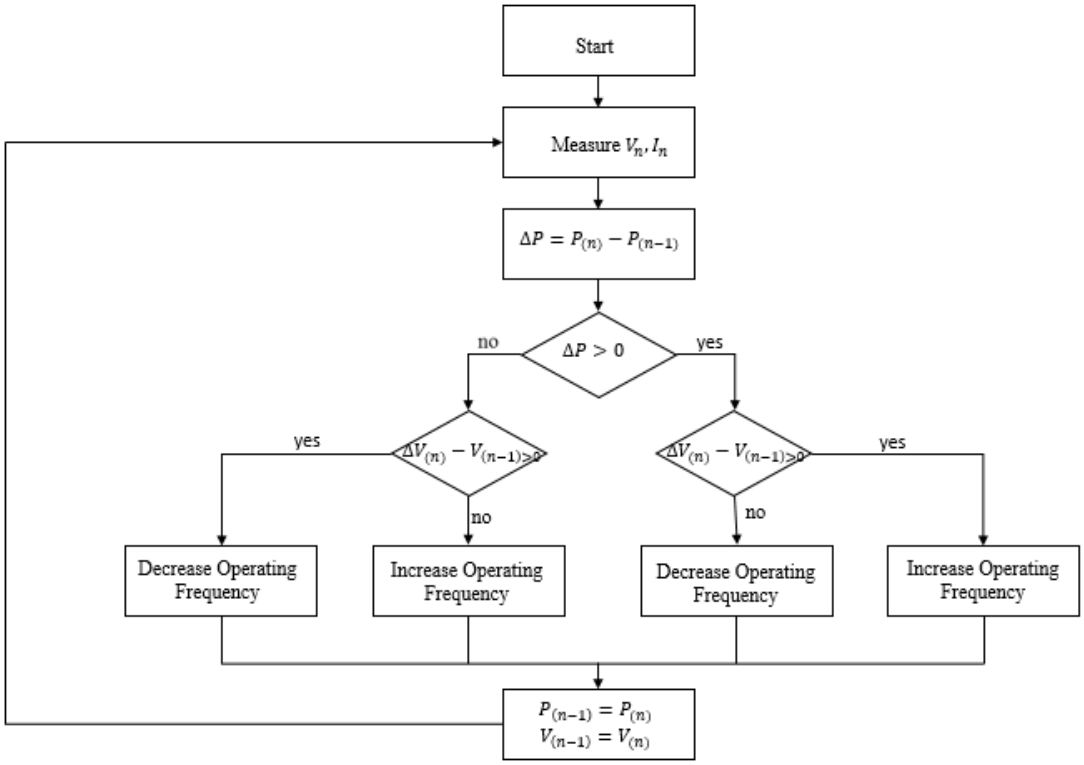

Figure 5.1 Flow chart of the frequency controlled load method

The complex and absolute impedances of the load at various operating frequency are calculated by using following equations and the results are given in Table 5.1.

$$X = 2\pi fL \quad \textbf{(5.1)}$$

$$Z = R + JX \quad \textbf{(5.2)}$$

$$|Z| = \sqrt{(R^2 + X^2)} \quad \textbf{(5.3)}$$

Table 5.1 Complex and absolute impedances of the DC motor at various frequency.

	Complex Impedance: $1.6 + J(f * 0.01319)\Omega$	Absolute Impedance
f=0Hz	1.6Ω	1.6Ω
f=100Hz	$1.6 + J1.3194\Omega$	2.07Ω
f=200H0z	$1.6 + J2.6389\Omega$	3.08Ω
f=400Hz	$1.6 + J5.2779\Omega$	5.51Ω
f=600Hz	$1.6 + J7.9168\Omega$	8.07Ω
f=800Hz	$1.6 + J10.555\Omega$	10.67Ω
f=1kHz	$1.6 + J13.194\Omega$	13.29Ω
f=2kHz	$1.6 + J26.389\Omega$	26.437Ω
f=4kHz	$1.6 + J52.778\Omega$	52.80Ω

When the motor reaches the optimum operating condition, the operating frequency is decreased/increased with small rates for oscillating around the MPPs. As a consequence, MPPT is accomplished efficiently by eliminating the power losses occur in DC-DC converter. However, the main disadvantage of the method is that the perturbation direction could be in wrong way for the conditions when the solar irradiance and temperature rates are not stable. Therefore, complex mathematic equations could be derived to determine the accurate way for the tracking.

5.3 The DC Motor Control Methods and MPPT Circuit

The PV array connected separately excited DC motor control and drive algorithm is much more different and complex than line connected DC motors. Traditional line connected separately excited DC motors could be controlled by switching a series starting resistor to armature circuit. Therefore, heavy starting current cannot burn the driver and motor windings. However, the PV array connected separately excited DC motor drive and control methods are based on the relation between the PV source and the load. Since, the PV array characteristics change with load and the intersection of load line with I-V curve of the PV array that determines operating point of PV array. Moreover, the intersection point affects

the DC motor operating voltage and current rates and therefore speed and torque characteristics are affected too.

First, the electrical and mechanical characteristics of the DC motor is determined with respect to the operating requirements of the centrifugal pump. The DC motor terminals are connected with the output of the designed PV array. Then the motor shaft is connected with the centrifugal pump by using an aluminum coupling. As a consequence, the electrical torque is converted to mechanical torque. The electrical and mechanical characteristics of the separately excited DC motor and the centrifugal pump are given below in Table 5.1 and Table 5.2.

Table 5.2 Separately excited DC motor data.

Rated Armature Voltage	220V
Armature Rated Voltage	220V
Armature Rated Current	23.5A
Armature Resistance	1.6ohm
Armature Inductance	2.1mH
Field Rated Voltage	220V
Field Rated Current	1.5A
Field Resistance	76ohm
Field Inductance	12.21H
Rated Motor Speed	3000rpm
Rated Motor Torque	15N-m
Efficiency	88%

Table 5.3 Centrifugal pump data.

Power	5HP
Flow Rate	42m3/h
Pressure Head	30m
Rated Speed	3000rpm

Secondly, the row and column of the PV array is designed by considering the electrical characteristics of the DC motor. Therefore, the PV array is consisted of 3 parallel and 8

series 24 pieces 230W polycrystalline Solar modules. Operating characteristics of the KDM 230P PV module is presented in Table 5.4.

Table 5.4: KDM 230P PV module operating characteristics.

Maximum Power Voltage (Vmp)	30V
Maximum Power Current (Imp)	7.67A
Open Circuit Voltage (Voc)	36V
Short Circuit Current (Isc)	8.59A
Maximum Power at STC(Pmax)	230W
Module Efficieny	14.1%
Operating Module Temperature	-40℃ - +85℃,
Maximum System Voltage	DC 1000V
Maximum Series Fuse Rating	15A
Power Tolerance	+3/-0%
Mechanical Loading	5400Pa
STC: Irradiance 1000W/m^2, module temperature 25℃, AM=1.5;	

When the irradiance level is at 1000 W/m^2, the Vmpp is 240V and Voc is 288V for the designed PV array. However, the electrical characteristics of the PV array change with various irradiance levels. PV module P-V graphic at various Solar irradiation is shown in Figure 5.2 and electrical characteristics of the PV module at various Solar irradiation levels are given in Table.5.5. If a reduction occurs in Solar irradiance then the operating voltage and power of the PV array will decrease. Therefore, the DC motor rated voltage is chosen low than Vmpp values at 1000W/m2 in order to tolerate the voltage difference for the low levels of the irradiance.

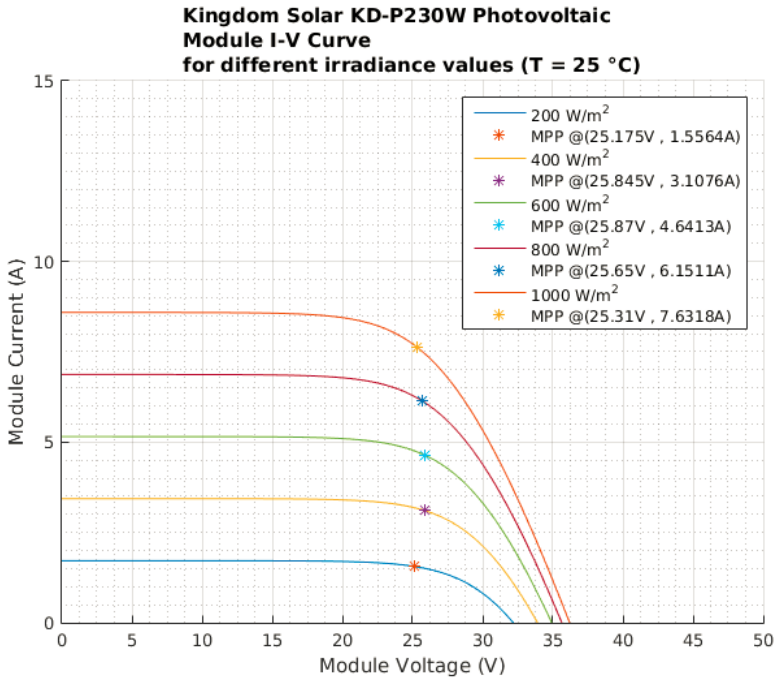

Figure 5.2 PV module P-V graphic at various Solar irradiation

Table 5.5 Electrical characteristics of the PV module at various Solar irradiation.

Solar Irradiation (W/m^2)	200W/m^2,	400W/m^2,	600W/m^2,	800W/m^2,	1000W/m^2,
Maximum Power (Pmax)	36W	76W	120W	180W	230W
Maximum Power Voltage (Vmp)	23.17V	24.54V	25.95V	27.85V	30V
Maximum Power Current (Imp)	1.58A	3.10A	4.64A	6.45	7.67A

Finally, the MPPT circuit that controls the DC motor and enables to deliver maximum power from the PV array by tracking the MPP, is designed and tested. The MPPT circuit for the proposed photovoltaic water pumping system is shown in Figure 5.3. The MPPT circuit is composed of two step down chopper circuits. To begin with, the DC motor field circuit is connected PV array and it will generate required magnetic fields to rotate armature. The DC motor is controlled by adjusting the duty cycle and frequency of the IGBT switches in step down chopper circuits. The pwm frequency is controlled by the

microcontroller and could be in range 100Hz – 2 kHz. After the current flows into the field winding, the magnetic field will produce the mechanical energy.

Secondly, another step down chopper circuit is used to control the armature circuit. For directly connected separately excited DC motors with PV source, the PV panel will operate in the short circuit current level since armature resistance is too low. Therefore, the DC motor will not accelerate. In the proposed PV water pumping system, the second step down chopper circuit is used to control the armature circuit. Switching frequency for the step down chopper circuit is around 100 Hz- 2 kHz and the duty cycle has increased from zero rate with %5 rates till the startup has finished and the back emf is increased. During the start up the switching frequency is adjusted to 200 Hz by the way the motor speed will be slow at startup. Since the low absolute impedance leads the operating point close to short circuit region in the PV I-V diagram. After the startup is finished and the back emf is rised, the MPPT unit starts to find the MPP locus of the PV array by changing the operating frequency. Consequently, the DC motor operates in steady state and the MPPT unit tracks the MPPs.

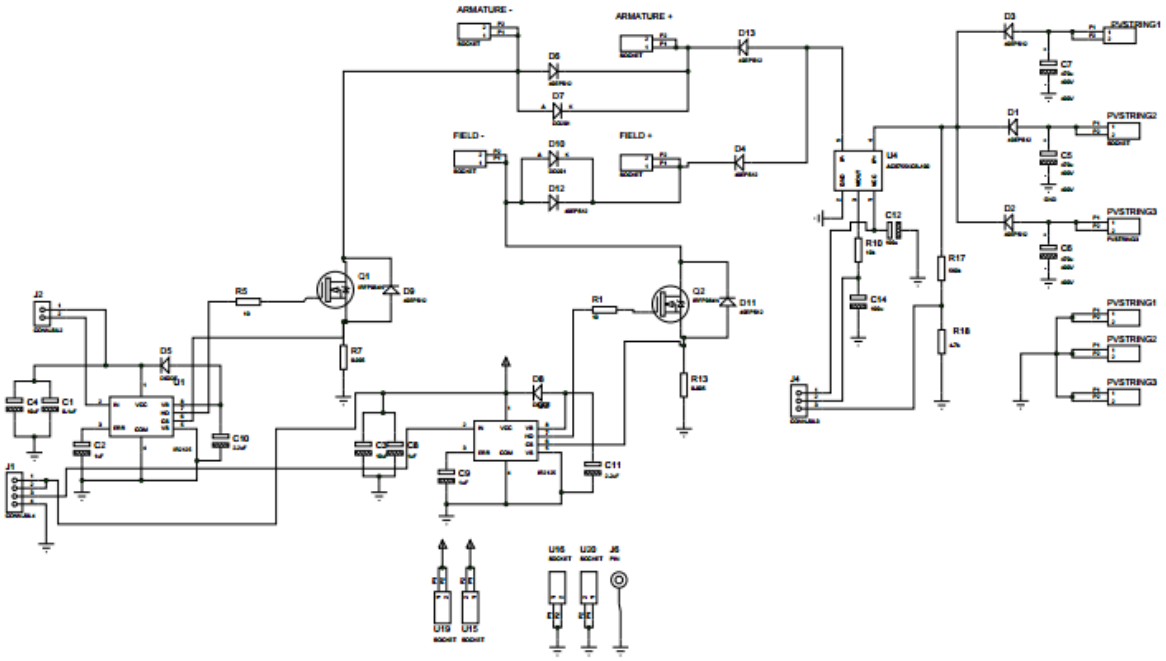

Figure 5.3 The MPPT circuit for the proposed photovoltaic water pumping system

5.4 Power Electronics for the Photovoltaic Water Pump

Power electronics for the proposed PV water pumping system includes safety designs: the overvoltage, overload and short circuit protections for the DC motor and switching devices in the step down chopper circuits. In addition, the snubber circuits are designed for the protection of both the load and switching elements. First of all, IGBT switches are defined and their operation characteristics in the step down chopper circuits are explored. Second, the gate driver specifications and operating characteristics are described and then the driver circuit is designed according to IGBTs and safety requirements. Finally, snubber circuits are designed for the safe operation of the IGBTs at turn off and turn on time.

5.4.1 IGBT Switches

IGBTs and gate drivers are the basic components in driver circuits. IGBT's turn on and turn of times have to be compatible with IGBT driver and snubber circuit designs. Since energy of both turn on snubber inductor and turn off snubber capacitor have to be discharged for the next period of IGBT turn on and turn off time. Moreover, IGBTs that have features of low turn on and turn off are more suitable for both snubber circuits and chopper DC motor drivers. In the step down chopper circuits the IGBT IXXH50N60C3D1 is used and the technical information of the IGBT is given in Table 5.6.

Table 5.6 Technical information of the IXXH50N60C3D1 IGBT.

Symbol	Test Conditions	Maximum Ratings
V_{CES}	$T_J = 25℃$ to $175℃$	600V
V_{GES} V_{GEM}	Continuous Transient	$\pm 20V$ $\pm 30V$
$V_{CE(sat)} \leq 2.30V$	$I_C = 36A, V_{GE} = \pm 20V$	2.30V
I_{C25} I_{C110} I_{F110} I_{CM}	$T_C = 25℃$ $T_C = 110℃$ $T_C = 110℃$ $T_C = 25℃$, 1ms	100A 50A 30A 200A
$t_{d(on)}$ t_{ri} $t_{d(off)}$ t_{fi}	Inductive load, $T_J = 25℃$ $I_C = 36A$ $V_{GE} = 15V$ $V_{CE} = 360V$ $R_G = 5\Omega$	24ns 40ns 62ns 42ns
Q_g Q_{ge} Q_{gc}	$I_C = 36A, V_{GE} = 15V$ $V_{CE} = 0.5xV_{CES}$	64nC 18nC 25nC

The power loss occur in IGBT is crucial for determining the heat sink design since if the cooling design is not efficient, then the limit operating temperature values of the IGBT could be exceeded. Also, the current limits of the IGBT decrease with the increasing temperature rates and that situation may lead the IGBT operate in outside of the SOA and RBSOA. The average power losses occur in the IGBT IXXH50N60C3D is calculated by using the following equation:

$$P_{loss} = 1/2\, xV_{CE}xI_{CE}xfx(t_{on} + t_{off}) \quad \textbf{(5.4)}$$

At 1000W/m^2 Solar irradiation the calculated average power dissipation in the IGBT for various switching frequency are given in Table 5.7. Consequently, an efficient and sustainable cooling design should be done in order to enable the IGBTs to operate safely.

Table 5.7 Power dissipation in the IGBT.

Frequency	f = 200Hz	f = 400Hz	f = 800Hz	f = 1kHz	f = 2kHz
IGBT: Power Dissipation	$36x10^{-3}$ W	$72x10^{-3}$ W	$145x10^{-3}$ W	$180x10^{-3}$ W	$360x10^{-3}$ W

5.4.2 IGBT Gate Drivers

IGBT gate drivers used in the step down chopper circuits are selected based turn on and turn off characteristics, delivered current rate for the IGBT and safety requirements. In the MPPT circuit, the selected IGBT gate driver is IR21215 and its technical information is given in Table 5.8.

Table 5.8 Technical information of IR2125.

Symbol	Definition	Min.	Max.	Units
V_B	High Side Floating Supply Voltage	$V_S + 12$	$V_S + 12$	V
V_S	High Side Floating Supply Voltage	-5	500	V
V_{HO}	High Side Floating Supply Voltage	V_S	V_B	V
V_{CC}	Logic Supply Voltage	0	18	V
V_{IN}	Logic Input Voltage	0	V_{CC}	V
V_{ERR}	Error Signal Voltage	0	V_{CC}	V
V_{CS}	Current Sense Signal Voltage	V_S	V_B	V
T_A	Ambient Temperature	-40	125	℃
t_{on}	Turn on Propagation Delay	-	200	ns
t_{on}	Turn off Propagation Delay	-	190	ns
t_{on}	Turn on Rise Time	--	60	ns
t_{on}	Turn off Fall Time		35	ns

First, IGBT gate driver selection is performed by matching between gate driver output current and the required current to drive the IGBT. The output current of the gate driver is related with the parameters: rise time, Vcc and load capacitance. Also, besides the power supply of the gate driver, the bypass capacitor enables to charge the gate capacitor quickly and it should be 50 times bigger than load capacitance. Moreover, it must be close to gate driver pins and the distance must be lower than 3 mm. In addition, the capacitors must be low ESR and ESL.

Secondly, IGBT gate resistor design is also one of the important subject that affects the switching time of the IGBT. Since when the IGBT turns off, the gate capacitor will discharge over the gate resistor and IGBT gate driver internal resistor. The gate resistor must be non-inductive carbon composition or metal film and since resistance tolerance must be around 1% for accurate gate drive calculations. Also, IGBT turn off time has to be short and since a fast and low voltage drop diode is needed. Therefore, an 18V 400mW zener diode is used parallel with the gate drive resistor. Moreover, a negative voltage can be applied to gate pins to shut down IGBT fast. Gate driver circuits used in proposed PV water pump is given in Figure 5.3. Power dissipation in the gate driver is calculated by using the following equations.

$$P_{dis.(on)} = \frac{D x R_{OH} x V_{cc} x Q_g x f_{sw}}{R_{OH} + R_{Gext} + R_{Gint}} \quad \textbf{(5.5)}$$

$$P_{dis.(off)} = \frac{(1-D) x R_{OL} x V_{cc} x Q_g x f_{sw}}{R_{OL} + R_{Gext} + R_{Gint}} \quad \textbf{(5.6)}$$

Where:

$P_{dis.(on)}$: Power dissipation for the turn on period

$P_{dis.(off)}$: Power dissipation for the turn off period

D: Duty cycle

R_{OH}: Output resistance of the driver when the output is high

R_{OL}: Output resistance of the driver when the output is low

R_{Gext} : The resistance externally serial with gate of IGBT

R_{Gint} : Internal mesh resistance of the IGBT

V_{cc}: Power supply voltage of the gate driver

Q_g: Gate charge of the IGBT

f_{sw}: Switching frequency

In the designed gate driver circuit R_{Gext}=10Ω, $R_{OH} = R_{OL} = 3.75Ω$, $V_{cc} = 15V$ and R_{Gint} is small and neglected. The power dissipation rates for the gate driver at various switching frequency are given in Table 5.9.

Table 5.9 Power dissipation in the gate driver.

Frequency	f = 200Hz	f = 400Hz	f = 800Hz	f = 1kHz	f = 2kHz
IGBT: Power Dissipation	$52x10^{-6}$	$104x10^{-6}$	$208x10^{-6}$	$260x10^{-6}$	$520x10^{-6}$

Finally, gate drive precautions must be considered carefully since internal resistance of the DC motor is so small and there may occur short circuit problem at start up. The basic and effective protections that enable IGBTs to operate in SOA and RBSOA are short circuit protections and desaturation detection circuits. Many gate driver ICs have internal overvoltage and short circuit protections. The IR2125 gate driver has a function of short circuit detection and the V_{CS} pin is used to sense current. In the gate driver circuit overvoltage is detected at the time V_{CS} pin reached 230mV and then and the gate driver will be in turn off state for a period. The situation will repeat until the overcurrent condition is finished. In the MPPT circuit, 46 A is determined for limiting the IGBT output current and 5mΩ current sense resistor is connected between V_{CS} and ground.

5.4.3 Snubber Circuits

Power semiconductors are exposed to stress in power electronic circuits during their operation. The stress may excess safe operating area of the semiconductor devices. In that condition either another semiconductor with an adequate safe operating area may be chosen or snubber circuits could be used to decrease the stress below the safe operating area. However, semiconductor with the broader range of safe operating area could be limited and therefore snubber circuit design must be developed for overcoming the stress over semiconductor devices.

The DC motor driver and the MPPT controller of the proposed off grid PV water pumping system need snubber circuits for the safety of IGBTs in step down DC chopper circuits.

The IGBTs are exposed to high stress when the IGBTs become on and off. Turn on and turn off I-V characteristics of the IGBTs are shown in Figure 5.4 [25].

There are three snubber circuits for the transistors and they expressed in following chapters.

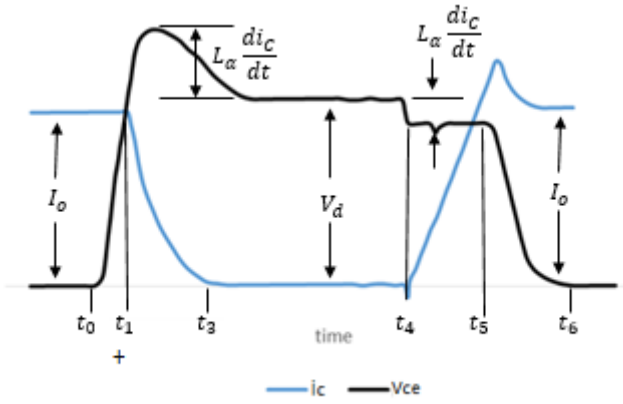

Figure 5.4 Current and voltage characteristics during turn on and turn off

5.4.3.1 *Turn off Snubber*

Turn off snubbers are used to decrease the stress over the IGBTs at turn off. At the beginning the transistor is on and its voltage V_{ce} is zero. During the switch is off the IGBT voltage begins to increase at $= t_0$. However, the IGBT current stays same until t_1 since the freewheeling diode begins to conduct at that time and the transistor current starts to decrease. At the time t_3 the IGBT current becomes zero and due to stray inductance transistor voltage exceeds V_d. The overvoltage is calculated by the following formula:

$$V_{ce} - V_d = -L\frac{di_c}{dt} \quad \textbf{(5.4)}$$

At turn off the IGBT voltage decreases with capacitor charging current in the RCD snubber circuit as shown in Figure 5.5.

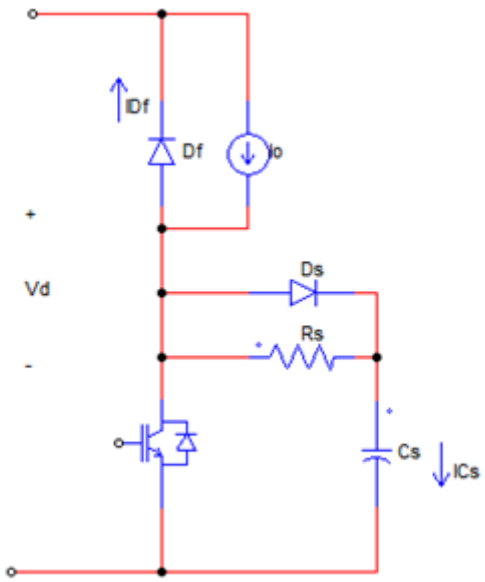

Figure 5.5 Turn off snubber circuit

Capacitor current is represented by the formula:

$$i_{Cs} = I_o \frac{t}{t_{fi}} \quad 0<t< t_{fi} \tag{5.5}$$

The capacitor voltage is equal to the transistor voltage and can be calculated by the following equation:

$$v_{Cs} = \frac{I_o t^2}{2C_s t_{fi}} \tag{5.6}$$

First, if the value of the capacitor is small than the snubber capacitor value then the capacitor reaches V_d quickly before the current becomes zero. Capacitor values smaller than snubber capacitor may not overcome stress enough.

Secondly, if $c_s = c_{s1}$ then the current value reaches to zero at time t_{fi} and capacitor voltage reaches V_d . The equation is expressed as:

$$C_{s1} = \frac{I_o t_{fi}}{2V_d} \tag{5.7}$$

Finally, for large values of C_{s1}, the transistor current reaches zero at time t_{fi}, however, the capacitor voltage reaches V_d after t_{fi}. In the armature and field chopper circuit design the snubber circuit is optimized by considering the transistor turn on time and position in the RBSOA. Also, the energy dissipated in snubber resistor is important for cooling design and its type. The energy is calculated by the formula:

$$W_R = \frac{C_s {V_d}^2}{2} \quad \textbf{(5.8)}$$

Moreover, snubber resistance is chosen by considering that snubber current is equal to reverse recovery current I_{rr} of freewheeling diode that is 20% of the output current and expressed by the formula:

$$\frac{V_d}{R_s} < I_{rr} = 0.2I_o \quad \textbf{(5.9)}$$

Finally, the snubber capacitor must be discharged during turn on time up to 0.1 V_d value and by using the following formula the necessary snubber capacitor and resistor values are reviewed with respect to turn on time [25].

$$V_{Cs} = V_d e^{-t/\tau_c} \quad \textbf{(5.10)}$$

$$t_{on\_state} > 2.3R_sC_s \quad \textbf{(5.11)}$$

Table 5.10 Turn off snubber circuit design.

Symbol	Test Conditions	200W/m^2	1000W/m^2	Units
$W_R = \frac{C_s {V_d}^2}{2}$	Solar Irradiance: 200W/m^2-1000W/m^2 f = 1Hz	8.5x10^{-6}	57.6x10^{-6}	W
C_s		0.5x10^{-9}	2x10^{-9}	F
R_s		195	52	Ω
t_{on_state} >		0.224x10^{-6}	0.239x10^{-6}	s

5.4.3.2 *Overvoltage Snubber*

Stray inductance causes overvoltage at turn off as shown in Fig. If the overvoltage stress is out of border of the SOA than the semiconductors may burn. Therefore by designing the overvoltage snubber that is shown in Figure 6, the overvoltage stress is reduced to tolerable rates.

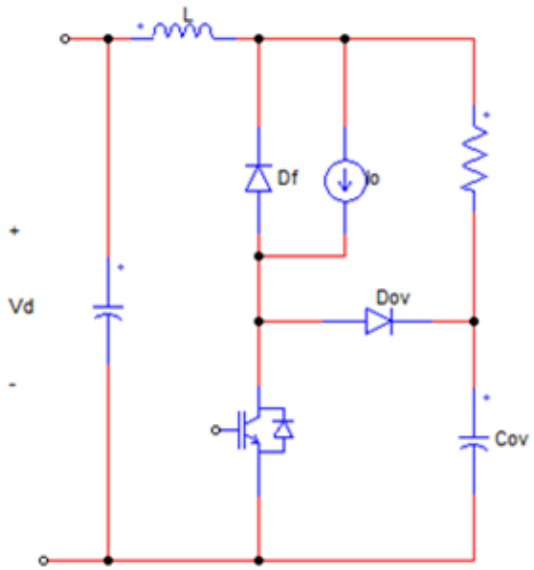

Figure 5.6 Overvoltage snubber circuit

By using the following energy formulas overvoltage capacitor rate is calculated:

$$\frac{C_{OV}\Delta V_{CE,max}{}^{2}}{2} = \frac{L_{\sigma}I_{o}{}^{2}}{2} \quad \textbf{(5.12)}$$

The overvoltage kV_d is used to calculate L by the equations:

$$kV_d = \frac{L_{\sigma}I_o}{t_{fi}} \quad \textbf{(5.13)}$$

Overvoltage snubber capacitor value for the armature circuit chopper circuit is calculated by estimating 0.1 V_d overvoltage and then following equation is derived [25].

$$C_{ov} = \frac{100kI_o t_{fi}}{V_d} \quad \textbf{(5.14)}$$

$$C_{ov} = 200kC_{s1} \quad \textbf{(5.15)}$$

The equation show that the overvoltage capacitor is much more than the snubber capacitor. The capacitor energy will dissipated in R_{ov} and therefore $R_{ov}C_{ov}$ discharge time must be enough for the capacitor voltage to decay zero. As a consequence, at the time next turn off, the overvoltage capacitor voltage should be discharged. To calculate overvoltage resistor value the following equation is used:

$$t_{on\_state} > 2.3R_sC_s \quad \textbf{(5.16)}$$

Table 5.11 Overvoltage snubber circuit design.

Symbol	Test Conditions	200W/m^2	1000W/m^2	Units
$W_C = \frac{C_{OV}\Delta V_{CE,max}{}^2}{2}$	Solar Irradiance: 200W/m^2 -1000W/m^2 Estimated Overvoltage =1V_d, f = 1Hz	1.7x10^{-3}	11.5x10^{-3}	W
kV_d		185	240	V
C_{ov}		100x10^{-9}	400x10^{-9}	F
L		195	52	H
t_{on_state} >		44.8x10^{-6}	47.8x10^{-6}	s

5.4.3.3 *Turn on Snubber*

Turn on switching losses at high switching frequency could be decreased by the turn on snubber circuit. Turn on snubber circuit could be serial with transistor or freewheeling diode as shown in Figure 5.7. Voltage reduction is calculated by the following formula:

$$\Delta V_{ce} = \frac{L_sI_o}{t_{ri}} \quad \textbf{(5.17)}$$

Where t_{ri} is the current rise time.

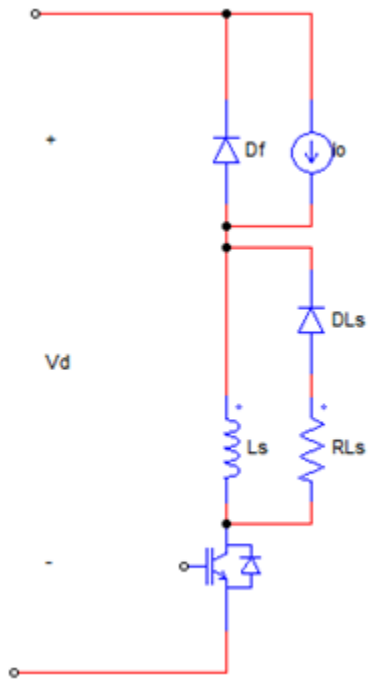

Figure 5.7 Turn on snubber circuit

During turn on the inductor stores energy and it will be dissipated in the snubber resistor when the IGBT turns off. The stored energy *W* is calculated by the following formula:

$$W = \frac{L_s {I_o}^2}{2} \tag{5.18}$$

Snubber resistor value is related with the overvoltage during the turn off. The overvoltage is estimated by the following formula:

$$\Delta V_{ce,max} = R_{Ls} I_o \tag{5.19}$$

Also, the snubber resistance value should allow inductor current to decay 0.1 I_o during the turn off time. The minimum off state value for the transistor is calculated by the following equations [25].

$$t_{off\_state} > 2.3 \frac{L_s}{R_{Ls}} \tag{5.20}$$

"t_{off_state}" is related with both snubber inductor and resistor. Larger inductor will reduce turn on voltage, however, it will increase turn off time. Thus, for the circuits in which switching frequency is high, a trade off may be needed. Also, the inductor energy is dissipated in snubber resistance and for the high switching frequency, cooling methods should be developed.

Table 5.12 Turn on snubber circuit design.

Symbol	Test Conditions	200W/m^2	1000W/m^2	Units
$W = \frac{L_s {I_o}^2}{2}$	Solar Irradiance: 200W/m^2 -1000W/m^2 $\Delta V_{ce,max}$=150V, f = 1Hz	$0.14x10^{-6}$	$0.66x10^{-6}$	W
R_{Ls}		31.65	3.45	Ω
L		$1.26x10^{-6}$	$0.25x10^{-6}$	H
t_{off_state} >		$91.56x10^{-9}$	$166.6x10^{-9}$	s

CHAPTER 6

CONCLUSION

6.1 Summary

In this thesis the photovoltaic centrifugal water pumping system including a separately excited DC motor is developed and DC motor controller with proposed MPPT method is analyzed. Safety precautions are applied for the motor controller and MPPT unit in order to force them to operate in SOA.

First of all, DC motor driver including armature and field step down DC chopper circuits are designed. Also, snubber circuits are designed and thus the switching IGBTs are worked in SOA and RBSOA. Moreover, gate driver circuits for armature and field step down DC chopper circuits are designed and tested. Since armature resistance is too low, during DC motor start up if the motor does not start to rotate and back emf stays at zero voltage then a high inrush current occurs. The inrush current would cause the transistor to be burn, however, the gate driver circuits are designed to limit the current of the transistors for operating them in SOA. The transistor is turned off for the current values above the limit value that is determined by the gate driver circuit.

Secondly, a new MPPT method is presented for load matching between PV array and DC motor. The load matching is accomplished by controlling switching frequency of IGBTs in the armature and field step down DC chopper circuits. By the way reading the voltage and current sensor, the switching frequency could be increased or decreased in order to track the MPPs. In the P-V graph increasing frequency will lead the tracking point to Voc direction and also decreasing frequency will move the operating point to the left side of the P-V graph.

Finally, the PV water pumping system with a DC motor connected centrifugal pump is tested in various irradiation and then the rpm, water pressure and flow rate data are recorded

and analyzed. Moreover, the DC motor start up software is tested and the rpm data is recorded.

To sum up, a photovoltaic water pumping system is designed and then working characteristic of the PV array with the separately excited DC motor connected centrifugal water pump is analyzed. Also, a new MPPT method for the PV water pump is developed and then the method is tested and the records are analyzed.

6.2 Difficulties and Future Research

Standalone photovoltaic water pumping systems include many research topics in terms of the relation among PV array and load characteristics. In addition, motor and pump types have different electrical and mechanical specifications and therefore combinations lead varying PV-load characteristic. Starting characteristic and steady state operation of the motor, pump types and MPPT methods are the basis for the researches. In the proposed PV water pumping system, difficulties related to environmental effects are observed such as changing irradiation, temperature and shadowing.

First of all, a separate DC bus could be used for supplying power to the field circuit. Since, an instant decrease in irradiation causes the PV array to operate in lower voltages and then the voltage reduction in the field circuit increase the motor rpm. Therefore, the motor torque will decrease. If a separate PV source or a battery connected field circuit is designed, controlling the motor would be easy.

Secondly, a tachometer sensor could be used to record the motor revolution data for the feedback circuit. Since, there may be a water and weather leakage in the centrifugal pump and it cannot work. Therefore, the motor behaves in no load operation and then the motor armature voltage increases with the higher voltage rates.

Finally, row and column numbers of the PV array are designed by considering electrical characteristics of the motor. In the PV water pumping system, a frequency control method is proposed and a step down DC chopper circuit is designed for MPPT tracking control method. For lower irradiance the PV operating voltage will decrease more than motor

steady state operating voltage. Therefore a boost converter could be used to increase PV output voltage. However, string designs of the PV array should be done by considering the boost converter increase rate, the steady state voltage and current of the motor, and the PV array output voltage rates at low level irradiance.

REFERENCES

[1] Sadasivam, P., Kumaravel, M., Vasudevan, K., Jhunjhunwala, A., *"Analysis of subsystems behaviour and performance evaluation of Solar photovoltaic powered water pumping system,"*, Photovoltaic Specialists Conference (PVSC), 2013 IEEE 39th , Vol., no., pp.2932-2937, 2013

[2] Chandel, S.S., Naik, M. N., Chandel, R., *"Review of Solar photovoltaic water pumping system technology for irrigation and community drinking water supplies*", Renewable and Sustainable Energy Reviews, Vol. 49, pp. 1084-1099, 2015

[3] Foster, R., & Cota, A., *"Solar Water Pumping Advances and Comparative Economics, Energy Procedia",* Volume 57, 2014, Pages 1431-1436

[4] Banu, I.V., Beniuga, R., Istrate, M., *"Comparative analysis of the perturb-and-observe and incremental conductance MPPT methods"*, Advanced Topics in Electrical Engineering (ATEE), 2013 8th International Symposium on , vol., no., pp.1-4, 23-25 May 2013

[5] Ceraolo, M., & Poli, D., *"Fundamentals of Electric Power Engineering: From Electromagnetics to Power Systems",* Wiley-IEEE Press, 2014.

[6] Appelbaum, J., *"The Quality of Load Matching in a Direct-Coupling Photovoltaic System"*, in Power Engineering Review, IEEE , vol.PER-7, no.12, pp.27-28, Dec. 1987

[7] Fam, W.Z., & Balachander, M.K., *"Dynamic performance of a DC shunt motor connected to a photovoltaic array"*, in Energy Conversion, IEEE Transactions on , vol.3, no.3, pp.613-617, Sep 1988

[8] Metwally, M.B., & Anis, W.R., *"Dynamic performance of directly coupled photovoltaic water pumping system using D.C. shunt motor, Energy Conversion and Management",* Volume 37, Issue 9, September 1996, Pages 1407-1416

[9] Kolhe, M., Joshi, J.C., Kothari, D.P., *"Performance analysis of a directly coupled photovoltaic water-pumping system"*, Energy Conversion, IEEE Transactions on , vol.19, no.3, pp.613-618, Sept. 2004

[10] Elgendy, M.A., Zahawi, B., Atkinson, D.J., *"Assessment of Perturb and Observe MPPT Algorithm Implementation Techniques for PV Pumping Applications"*, Sustainable Energy, IEEE Transactions on , vol.3, no.1, pp.21-33, Jan. 2012

[11] Ouachani, I., Rabhi, A., El Hajjaji, A., Tidhaf, B., Zouggar, S., *"A robust control method for a DC motor-based photovoltaic pumping"*, in Systems and Control (ICSC), 2013 3rd International Conference on , vol., no., pp.720-726, 29-31 Oct. 2013

[12] Jaziri, S., & Jemli, K., *"Optimization of a photovoltaic powered water pumping system"*, Control, Decision and Information Technologies (CoDIT), 2013 International Conference on , vol., no., pp.422-428, 6-8 May 2013

[13] Chauhan, J., Chauhan, P., Maniar, T., Joshi, A., *"Comparison of MPPT algorithms for DC-DC converters based photovoltaic systems"*, Energy Efficient Technologies for Sustainability (ICEETS), 2013 International Conference on , vol., no., pp.476-481, 10-12 April 2013

[14] Nayar, C.V., Islam, S.M., Dehbonei, H., Tan, K., *"Power Electronics Handbook"*, Academic Press, Burlington, 2007.

[15] Galad, M., & Spanik, P., "Design of photovoltaic Solar cell model for stand-alone renewable system," ELEKTRO, 2014, vol., no., pp.285-288, 19-20 May 2014

[16] Bundalo, D., Bundalo, Z., Bundalo, Z., *"Temperature characteristics and energy efficiency of Solar cells and Solar modules"*, Embedded Computing (MECO), 2012 Mediterranean Conference on , vol., no., pp.288-291, 19-21 June 2012

[17] El-Hawary, M., *"Principles of Electric Machines with Power Electronic Applications"*, Wiley-IEEE Press, 2002

[18] Beloiu, R., "*Dynamic determination of DC motor parameters - Simulation and testing"*, Electronics, Computers and Artificial Intelligence (ECAI), 2014 6th International Conference on , vol., no., pp.13-18, 23-25 Oct. 2014

[19] Hoque, M.A., Zaman, M.R., Rahman, M.A., *"Artificial neural network based permanent magnet DC motor drives"*, Industry Applications Conference, 1995. Thirtieth IAS Annual Meeting, IAS '95., Conference Record of the 1995 IEEE , vol.1, no., pp.98-103 vol.1, 8-12 Oct 1995

[20] Karady, G., & Holbert, K., *"Electrical Energy Conversion and Transport: An Interactive Computer-Based Approach"*, Wiley-IEEE Press, 2005.

[21] Krause, P., Wasynczuk, O., Pekarek, S., *"Electromechanical Motion Devices"*, Wiley-IEEE Press, 2012

[22] Oise, I.M., Diala, U.H., Ezeh, G.N., Opara, R., *"Evaluation of transient response of a separately excited DC motor under no-load condition"*, Emerging & Sustainable Technologies for Power & ICT in a Developing Society (NIGERCON), 2013 IEEE International Conference on , vol., no., pp.258-262, 14-16 Nov. 2013

[23] Chau, K.T., *"Electric Vehicle Machines and Drives: Design, Analysis and Application"*, 1, Wiley-IEEE Press, 2015, pp.375 [24]

[24] Hughes, A., & Drury, B., *"Electric Motors and Drives: Fundamentals, Types and Applications",* Elsevier, Oxford, 2013.

[25] Mohan, N., Undeland, M.T., Robbins, W.P., *"Power Electronics: Converters, Applications, and Design"*, Wiley, New York, 1995.

[26] Castaner, L., & Sivestre, S., *"Modelling Photovoltaic Systems Using PSpice"*, Wiley, 2006.

[27] Esram, T.; Chapman, P.L., "Comparison of Photovoltaic Array Maximum Power Point Tracking Techniques," Energy Conversion, IEEE Transactions on , vol.22, no.2, pp.439-449, June 2007

[28] Chauhan, J., Chauhan, P., Maniar, T., Joshi, A., *"Comparison of MPPT algorithms for DC-DC converters based photovoltaic systems"*, Energy Efficient Technologies for Sustainability (ICEETS), 2013 International Conference on , vol., no., pp.476-481, 10-12 April 2013

[29] Zhang, Hui, Hong Ji, Jing Ren, Lin Shan, Yongjun Gao, *"Research on MPPT control and implementation method for photovoltaic generation system and its simulation"*, Power Electronics and Motion Control Conference, 2009. IPEMC '09. IEEE 6th International , vol., no., pp.2108-2112, 17-20 May 2009

[30] Zhang, X., Zha, L., Liu, F., Tao, L., Chen,W., *"The analysis of power loss caused by the truncation error of MPPT algorithms"*, Power Electronics for Distributed Generation Systems (PEDG), 2010 2nd IEEE International Symposium on , vol., no., pp.7-11, 16-18 June 2010

[31] Abderezak, L., Aissa, B., Hamza, S., *"Comparative study of three MPPT algorithms for a photovoltaic system control"*, Information Technology and Computer Applications Congress (WCITCA), 2015 World Congress on , vol., no., pp.1-5, 11-13 June 2015

[32] Roberto, F., & Leva, S., *"Energy comparison of MPPT techniques for PV Systems"*, WSEAS transactions on power systems 3.6 (2008): 446-455.

[33] Elgendy, M.A., Zahawi, B., Atkinson, D.J., Giaouris, D., *"Dynamic behaviour of DC motor-based photovoltaic pumping systems under searching MPPT algorithms"*, Power Engineering, Energy and Electrical Drives, 2009. POWERENG '09. International Conference on , vol., no., pp.413-418, 18-20 March 2009

[34] Harvie, D., & Rajakaruna, S., *"A hardware implementation and analysis of testing MPPT algorithms on PV modules"*, Power Engineering Conference (AUPEC), 2014 Australasian Universities, vol., no., pp.1-6, Sept. 28 2014-Oct. 1 2014

[35] Martin, A.D., & Vazquez, J.R., *"MPPT algorithms comparison in PV systems: P&O, PI, neuro-fuzzy and backstepping controls"*, Industrial Technology (ICIT), 2015 IEEE International Conference on , vol., no., pp.2841-2847, 17-19 March 2015

[36] Khaehintung, N., Wiangtong, T., Sirisuk, P., *"FPGA Implementation of MPPT Using Variable Step-Size P&O Algorithm for PV Applications"*, Communications and Information Technologies, 2006. ISCIT '06. International Symposium on, vol., no., pp.212-215, Oct. 18 2006-Sept. 20 2006

[37] Cristian, H.I., & Raducu, M., *"Performance comparison of three MPPT algorithms: AESC, mESC and P&O"*, in Electronics, Computers and Artificial Intelligence (ECAI), 2015 7th International Conference on , vol., no., pp.S-35-S-42, 25-27 June 2015

[38] Sahu, T.P., & Dixit, T.V., *"Modelling and analysis of Perturb & Observe and Incremental Conductance MPPT algorithm for PV array using Ċuk converter"*, Electrical, Electronics and Computer Science (SCEECS), 2014 IEEE Students' Conference on , vol., no., pp.1-6, 1-2 March 2014

[39] Kollimalla, S.K., & Mishra, M.K., *"A Novel Adaptive P&O MPPT Algorithm Considering Sudden Changes in the Irradiance"*, Energy Conversion, IEEE Transactions on , vol.29, no.3, pp.602-610, Sept. 2014

[40] Aashoor, F.A.O., & Robinson, F.V.P., *"A variable step size perturb and observe algorithm for photovoltaic maximum power point tracking"*, Universities Power Engineering Conference (UPEC), 2012 47th International, vol., no., pp.1-6, 4-7 Sept. 2012

[41] Kollimalla, S.K., & Mishra, M.K., *"Variable Perturbation Size Adaptive P&O MPPT Algorithm for Sudden Changes in Irradiance"*, Sustainable Energy, IEEE Transactions on , vol.5, no.3, pp.718-728, July 2014

[42] Chairma Lakshmi, K.R., Shankar, K., Thangaraj, M., Abudhahir, A., *"Performance analysis of MPPT algorithms for enhancing the efficiency of SPV power generation system: A simulation study"*, Emerging Trends in VLSI, Embedded System, Nano Electronics and Telecommunication System (ICEVENT), 2013 International Conference on , vol., no., pp.1-5, 7-9 Jan. 2013

[43] Gaga, A., Errahimi, F., Es-Sbai, N., *"Design and implementation of MPPT Solar system based on the enhanced P&O algorithm using Labview"*, Renewable and Sustainable Energy Conference (IRSEC), 2014 International , vol., no., pp.203-208, 17-19 Oct. 2014

[44] ChittiBabu, B., Samantaray, S.R., Saraogi, N., Ashwin Kumar, M.V., Sriharsha, R., Karmaker, S., *"Synchronous Buck Converter based PV Energy System for Portable Applications"*, Students' Technology Symposium (TechSym), 2011 IEEE , vol., no., pp.335-340, 14-16 Jan. 2011

BIOGRAPHY

Mustafa Emre Aras was born on October 30, 1987, in Kayseri, Turkey. He received the Bachelor of Science Degree from İhsan Doğramacı Bilkent University, Ankara, Turkey in 2010. He worked in Turkey in the areas of the power electronics, photovoltaic energy applications, embedded system and DC motor driver units. He applied for his proposed PV water pumping system and patented it in 2013. His career objectives are to continue power electronics researches on the Photovoltaic applications.

Appendix A Equations

A.2.1 $I = I_{ph} - I_d$

A2.2 $I_d = I_o\left(e^{\frac{qV_d}{nkT}} - 1\right)$

A.2.3 $I_o = I_{sc}\left(\frac{T}{T_{ref}}\right)^3 e^{\frac{qE_g}{nk}\left(\frac{1}{T_{ref}} - \frac{1}{T}\right)}$

A2.4 $I_{ph} = \frac{\emptyset}{\emptyset_{ref}}\left(I_{scr} + \alpha_{isc}(T - T_{ref})\right)$

A.3.1 $\emptyset_f = k_f I_f$

A.3.2 $T_{em} = k_t \emptyset_f i_a$

A.3.3 $e_a = k_e \emptyset_f \omega_m$

A.3.4 $v_t = R_a i_a + L_a \frac{di_a}{dt} + e_a$

A.3.5 $v_f = R_f i_f + L_f \frac{di_f}{dt}$

A.3.6 $e_a = K i_f \omega_m$

A.3.7 $T_{em} = J\frac{d\omega}{dt} + D\omega_m + T_L$

A.3.8 $V_t = R_a I_a + E_a$

A.3.9 $V_f = R_f I_f$

A.3.10 $E_a = K I_f \omega_m$

A.3.11 $T_{em} = J\omega_m + T_L$

A.3.12 $\omega_m = \frac{1}{k_e \emptyset_f}\left(V_t - \frac{R_a}{k_t \emptyset_f} T_{em}\right)$

A.3.13 $T_{em} = k_t I_a$

A.3.14 $E_a = k_E \omega_m$

A.3.15 $i = \left(\frac{V_2 - V_1}{R}\right) e^{-t/\tau}$

A.3.16 $\tau = \frac{RJ}{k^2}$

A.3.17 $\tau_a = \frac{L}{R}$

A.3.18 $t_L = A + B\omega^2$

A.3.19 $H = A_1 S^2 + B_1 SQ + C_1 Q^2$

A.4.1 $\frac{dP}{dV} = 0$

A.4.2 $\frac{dP}{dV} > 0$

A.4.3 $\frac{dP}{dV} < 0$

A.4.4 $\frac{dP}{dV} = \frac{d(VxI)}{dV} = I\frac{dV}{dV} + V\frac{dI}{dV} = I + V\frac{dI}{dV}$

A.4.5 $I + V\frac{dI}{dV} = 0$

A.4.6 $\frac{dI}{dV} = -\frac{I}{V}$

A.4.7 $I + V\frac{dI}{dV} > 0$

A.4.8 $\frac{dI}{dV} > -\frac{I}{V}$

A.4.9 $I + V\frac{dI}{dV} < 0$

A.4.10 $\frac{dI}{dV} < -\frac{I}{V}$

A.4.11 $(V_s - V_o)DT = -V_o(1-D)T$

A.4.12 $V_o = DV_s$

A.4.13 $L_b = \frac{(1-D)R}{2f}$

A.4.14 $C_{min} = \frac{(1-D)V_o}{8V_r Lf^2}$

A.4.15 $V_s DT = (V_o - V_s)(1-D)T$

A.4.16 $\frac{V_o}{V_s} = \frac{1}{1-D}$

A.4.17 $L_b = \frac{(1-D)^2 DR}{2f}$

A.4.18 $C_{min} = \frac{DV_o}{V_r RF}$

A.4.19 $V_s DT = -V_o(1-D)T$

A.4.20 $\frac{V_o}{V_S} = -\frac{D}{1-D}$

A.4.21 $L_b = \frac{(1-D)^2 R}{2f}$

A.4.22 $C_{min} = \frac{DV_o}{V_r RF}$

A.4.23 $I_{L2}DT = I_{L1}(1-D)T$

A.4.24 $\frac{V_o}{V_S} = -\frac{D}{1-D}$

A.4.25 $L_{b1} = \frac{(1-D)R}{2Df}$

A.4.26 $L_{b2} = \frac{(1-D)R}{2Df}$

A.4.27 $C_{min} = \frac{(1-D)V_o}{8V_r L_2 f^2}$

A.5.1 $X = 2\pi fL$

A.5.2 $Z = R + JX$

A.5.3 $|Z| = \sqrt{(R^2 + X^2)}$

A.5.4 $P_{loss} = 1/2\, xV_{CE}xI_{CE}xfx(t_{on} + t_{off})$

A5.5 $P_{dis.(on)} = \frac{DxR_{OH}xV_{cc}xQ_g xf_{sw}}{R_{OH}+R_{Gext}+R_{Gint}}$

A.5.6 $P_{dis.(off)} = \frac{(1-D)xR_{OL}xV_{cc}xQ_g xf_{sw}}{R_{OL}+R_{Gext}+R_{Gint}}$

A.5.7 $V_{ce} - V_d = -L\frac{di_c}{dt}$

A.5.5 $i_{Cs} = I_o \frac{t}{t_{fi}}$ $0<t< t_{fi}$

A.5.6 $v_{Cs} = \frac{I_o t^2}{2C_s t_{fi}}$

A.5.7 $C_{s1} = \frac{I_o t_{fi}}{2V_d}$

A.5.8 $W_R = \frac{C_s {V_d}^2}{2}$

A.5.9 $\frac{V_d}{R_s} < I_{rr} = 0.2I_o$

A.5.10 $V_{Cs} = V_d e^{-t/\tau_c}$

A.5.11 $t_{on\_state} > 2.3R_s C_s$

A.5.12 $\frac{C_{OV}\Delta V_{CE,max}{}^2}{2} = \frac{L_\sigma {I_o}^2}{2}$

A.5.13 $kV_d = \frac{L_\sigma I_o}{t_{fi}}$

A.5.14 $C_{ov} = \frac{100kI_o t_{fi}}{V_d}$

A.5.15 $C_{ov} = 200kC_{s1}$

A.5.16 $t_{on\_state} > 2.3R_sC_s$

A.5.17 $\Delta V_{ce} = \frac{L_s I_o}{t_{ri}}$

A.5.18 $W = \frac{L_s {I_o}^2}{2}$

A.5.19 $\Delta V_{ce,max} = R_{Ls}I_o$

A.5.20 $t_{off\_state} > 2.3\frac{L_s}{R_{Ls}}$

Appendix B Figures

B.2.1

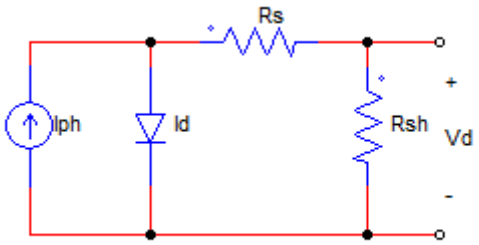

Figure 2.1 Equivalent circuit of PV Cell

B.2.2

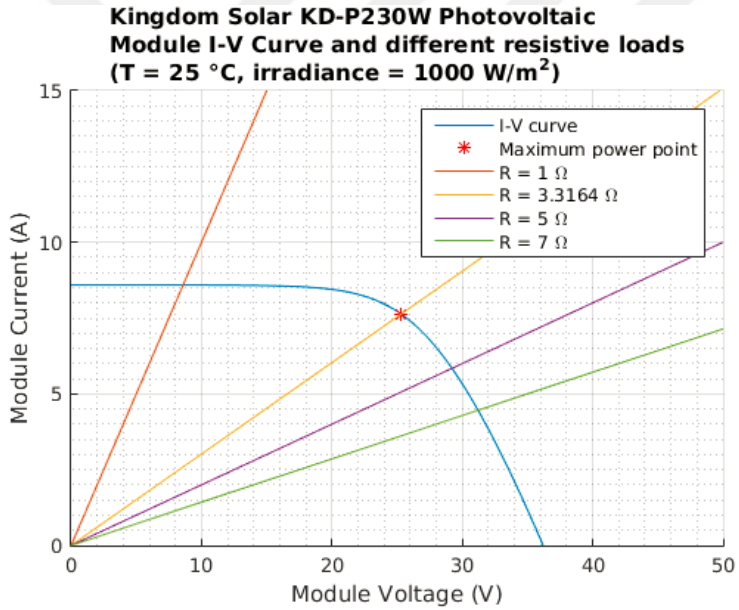

Figure 2.2 I-V curves of KDM 230P PV module and various load connections

B.2.3

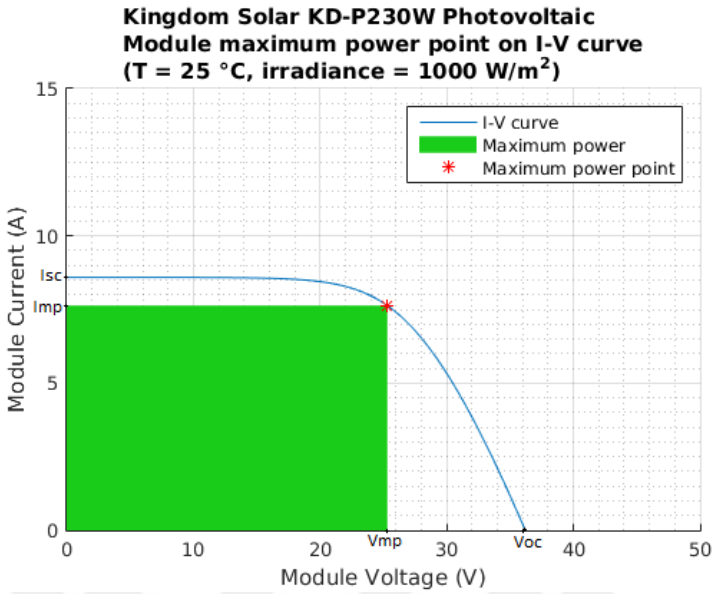

Figure 2.3 I-V curves of KDM 230P PV module and specific operating points

B.2.4

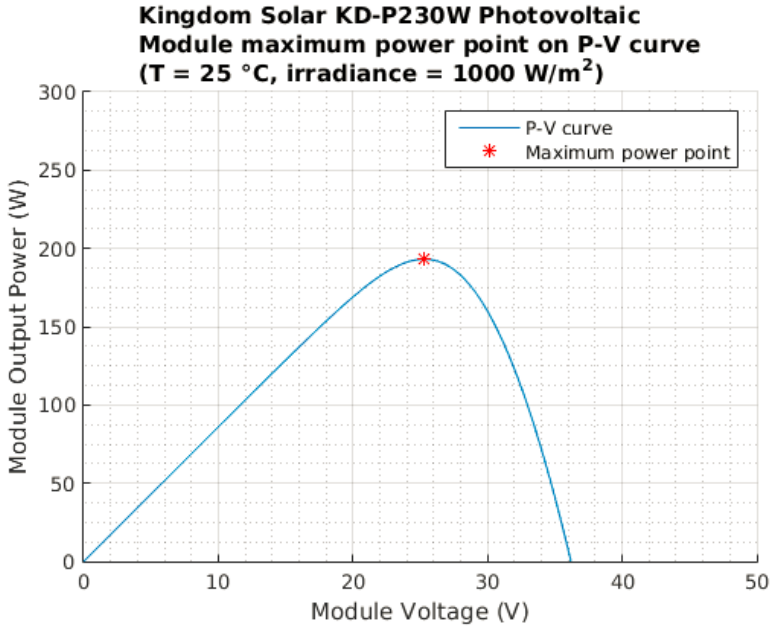

Figure 2.4 P-V characteristics of the KDM 230P PV module

B.2.5

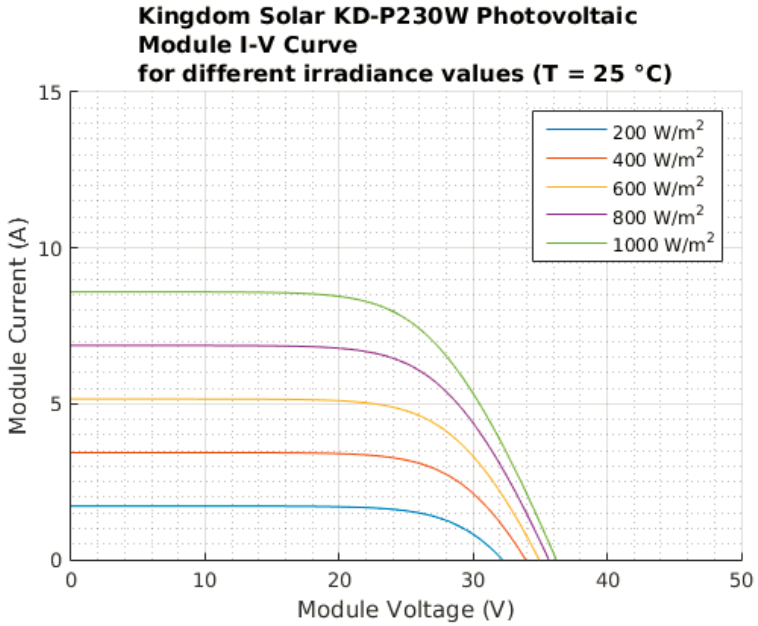

Figure 2.5 PV module I-V graphic at various Solar irradiation

B.2.6

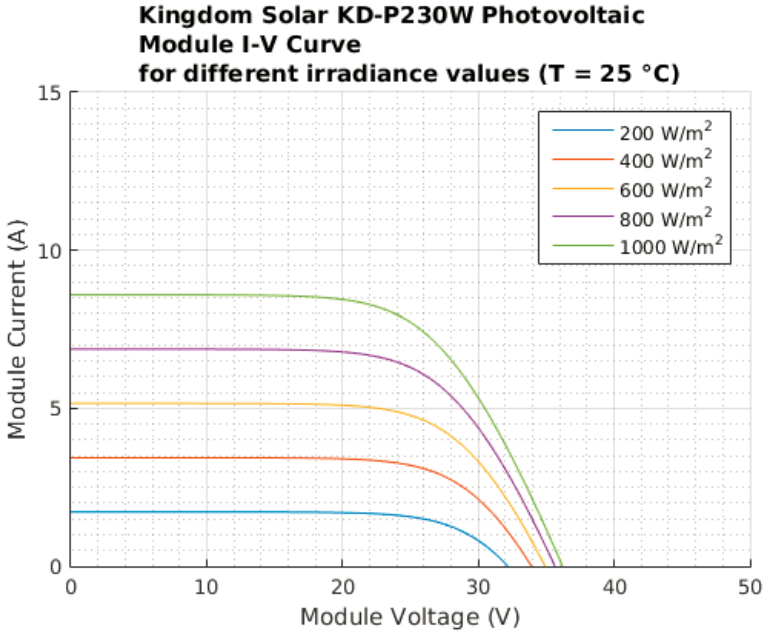

Figure 2.6 PV module P-V graphic at various Solar irradiation

B.2.7

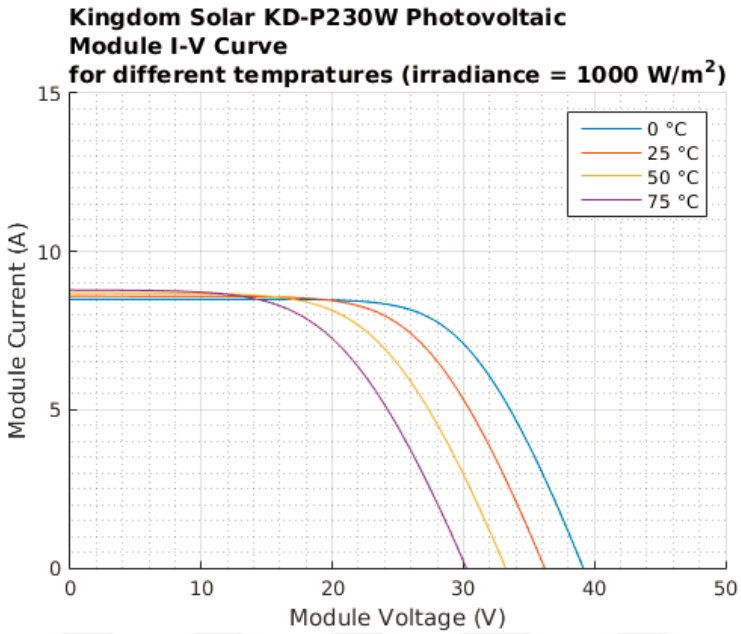

Figure 2.7 PV module I-V graphic at various temperature rates

B.3.1

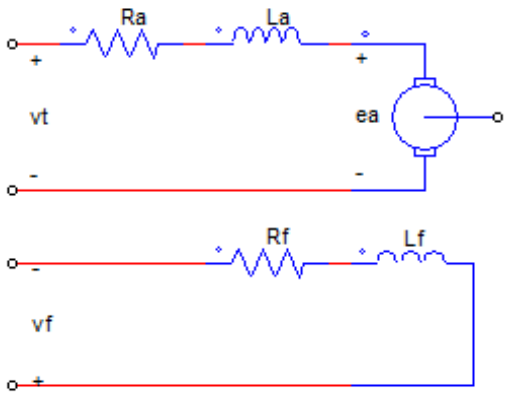

Figure 3.1 Equivalent circuit of the separately excited DC motor

B.3.2

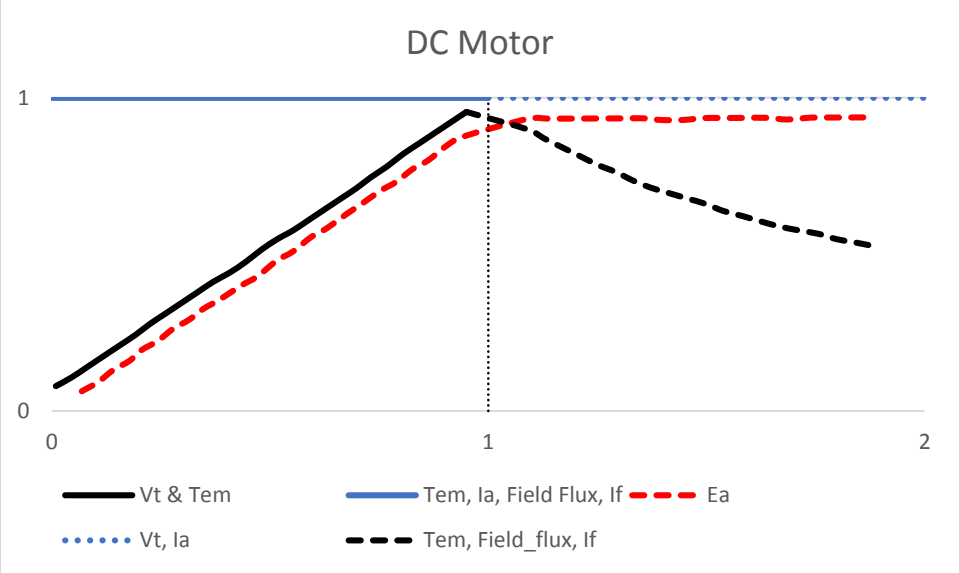

Figure 3.2 Steady state operation in the torque-speed plane

B.3.3

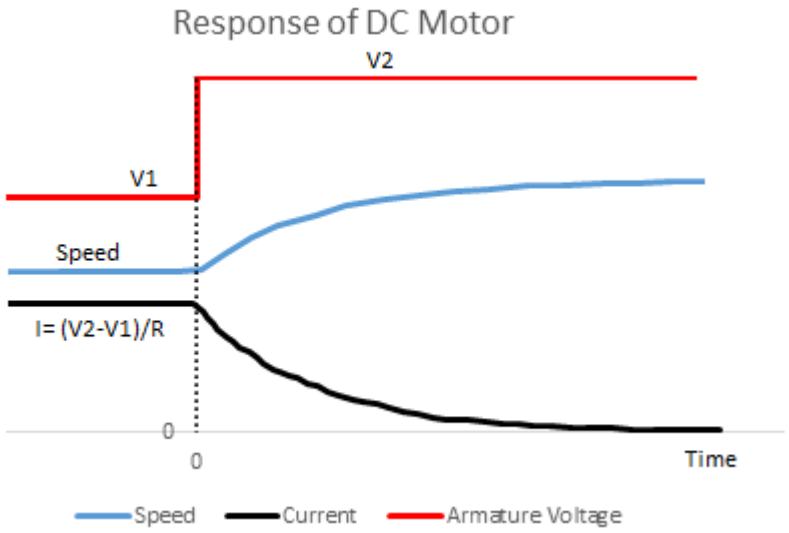

Figure 3.3 Step increase characteristics of the DC motor

B.4.1

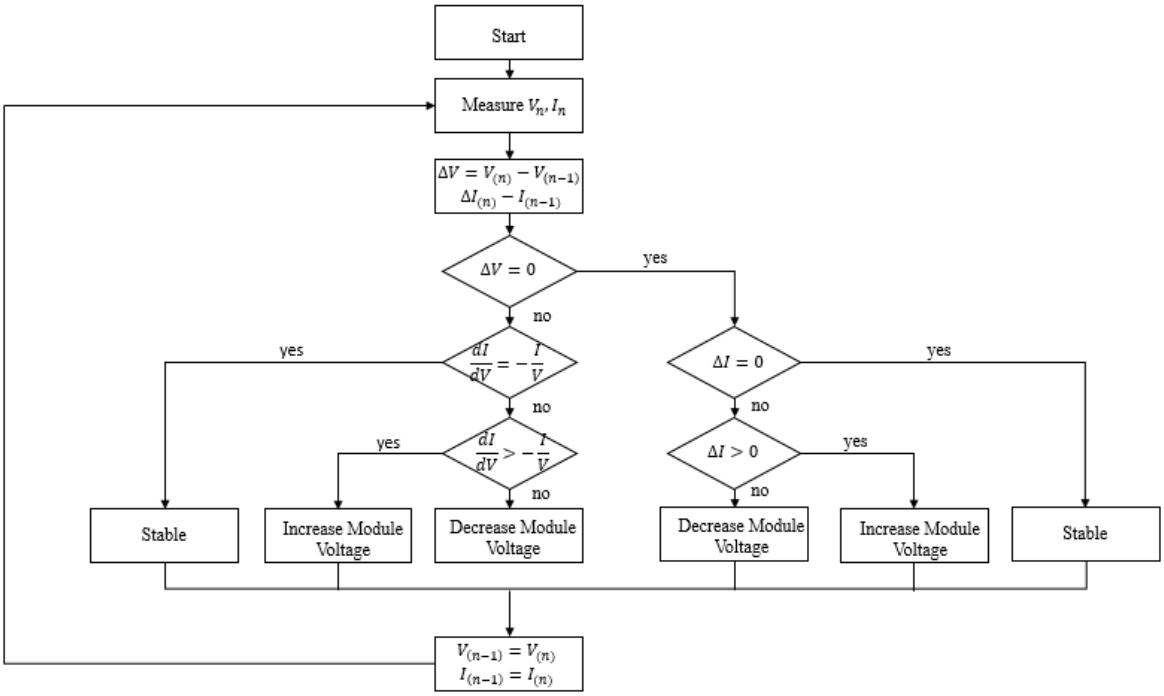

Figure 4.1 Flow chart of the ICT method

B.4.2

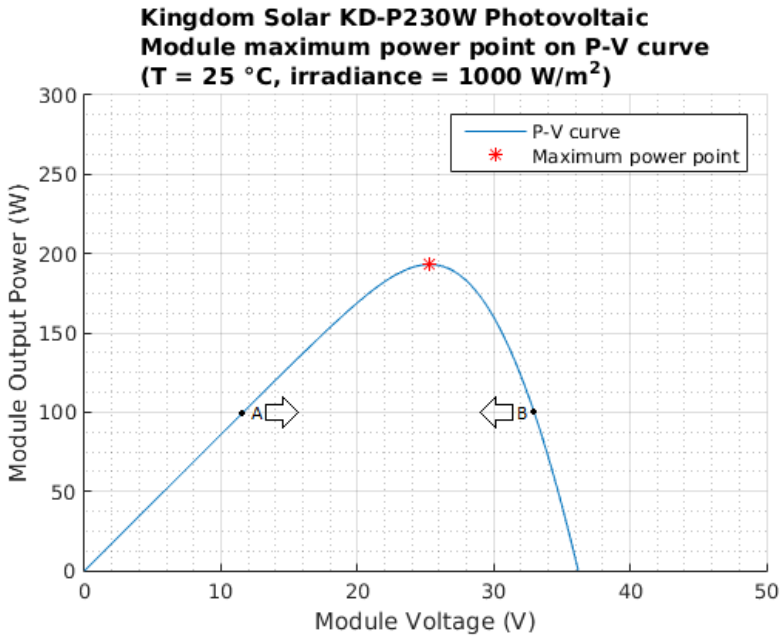

Figure 4.2 The PAO method and its operating paths

B.4.3

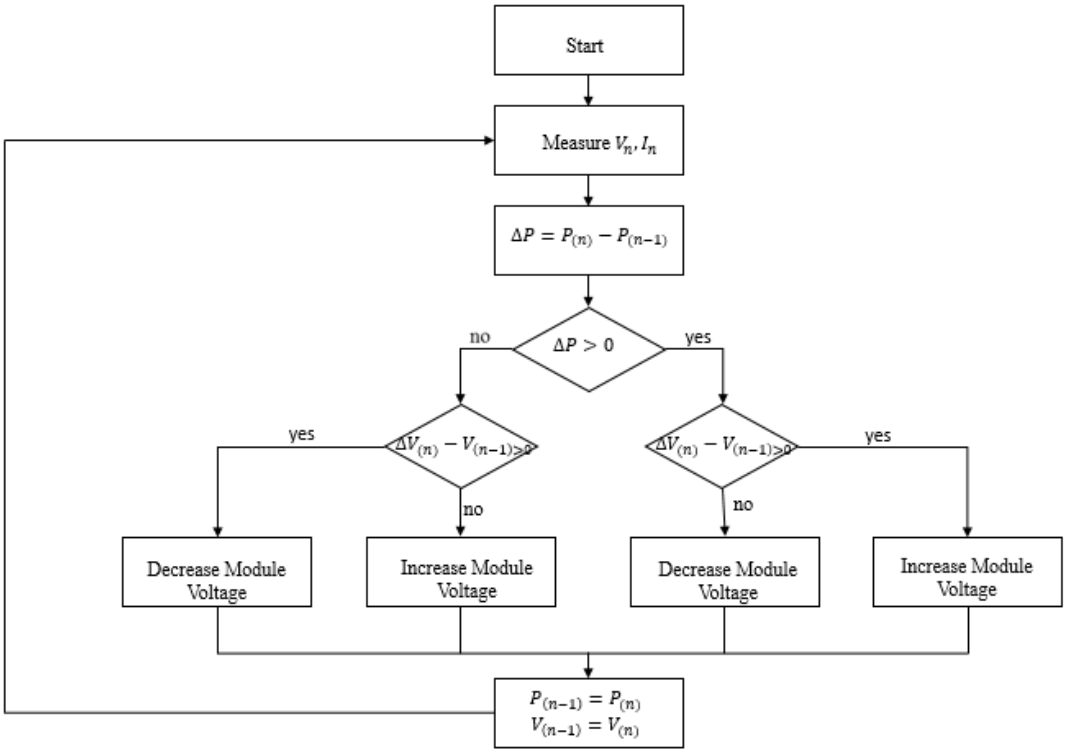

Figure 4.3 Flowchart of the PAO method

B.4.4

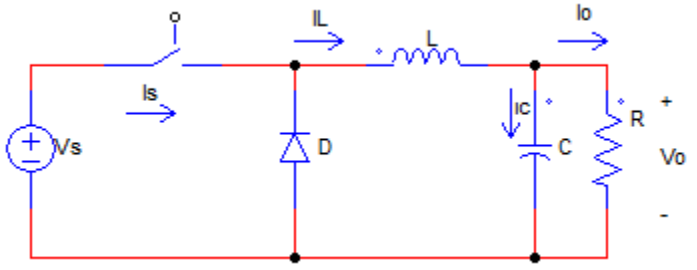

Figure 4.4 Step Down converter

B.4.5

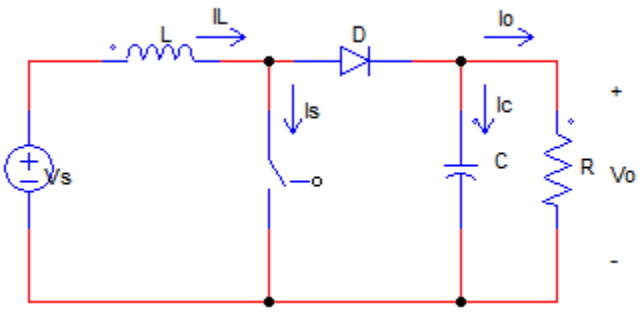

Figure 4.5 Step Up converter

B.4.6

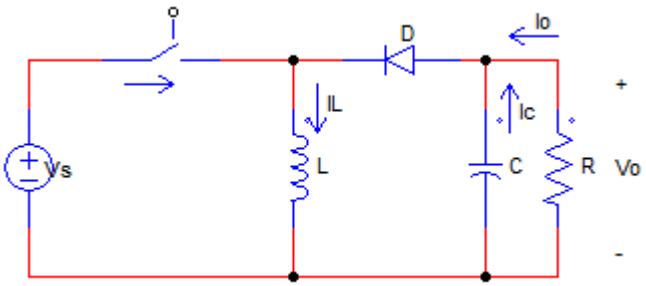

Figure 4.6 Buck Boost Converter

B.4.7

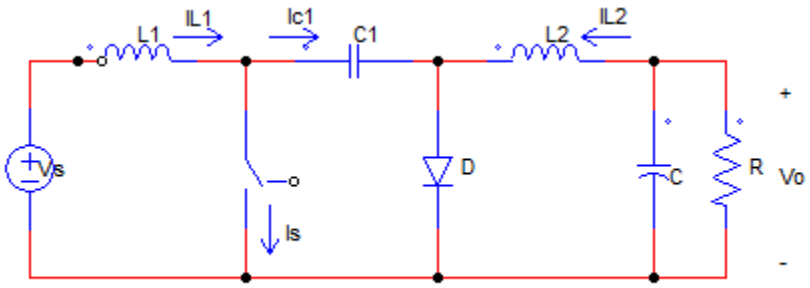

Figure 4.7 Cúk Converter

B.5.1

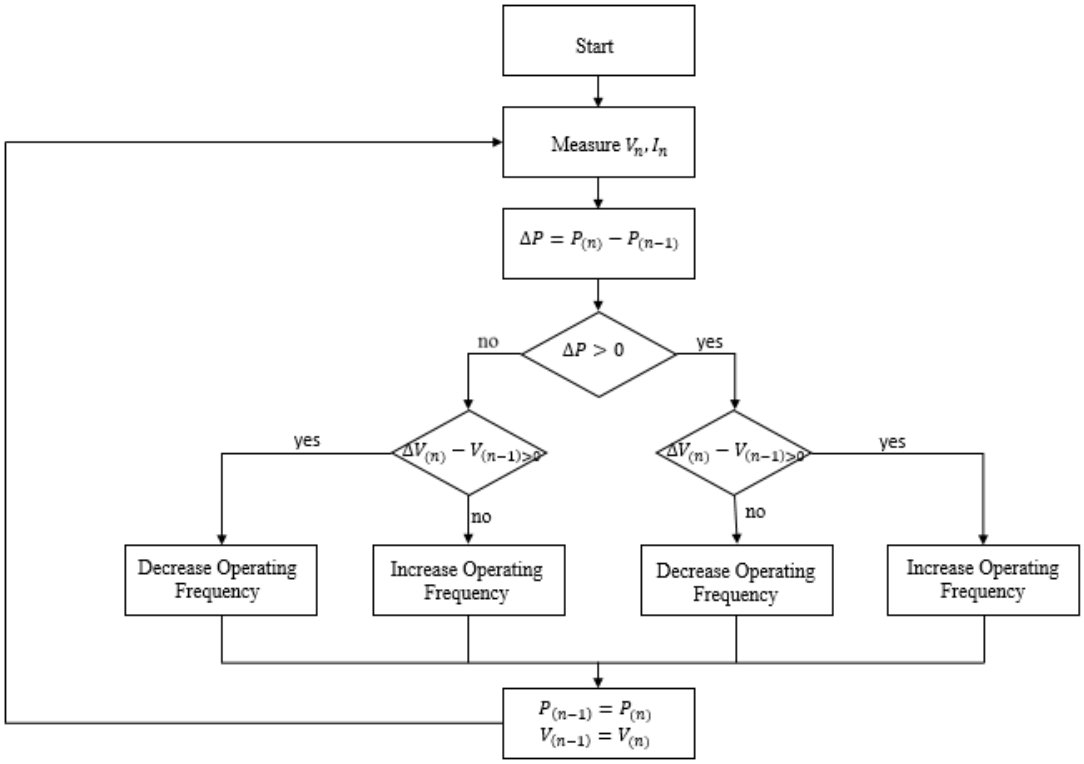

Figure 5.1 Flow chart of the frequency controlled load method

B.5.2

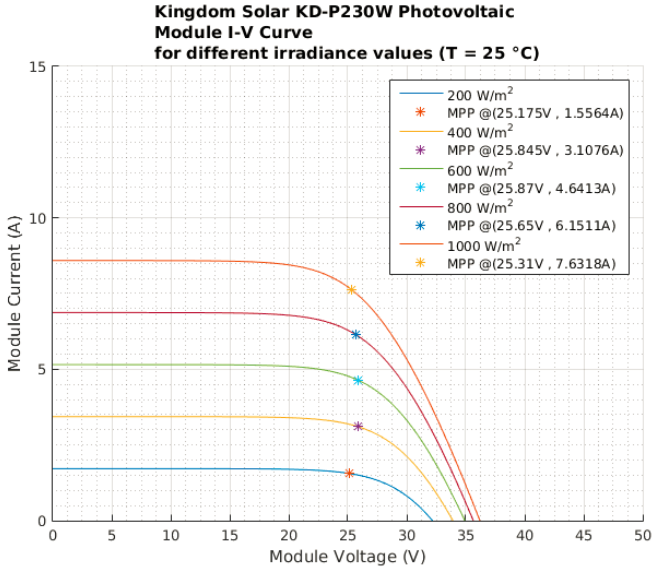

Figure 5.2 PV module P-V graphic at various Solar irradiation

B.5.3

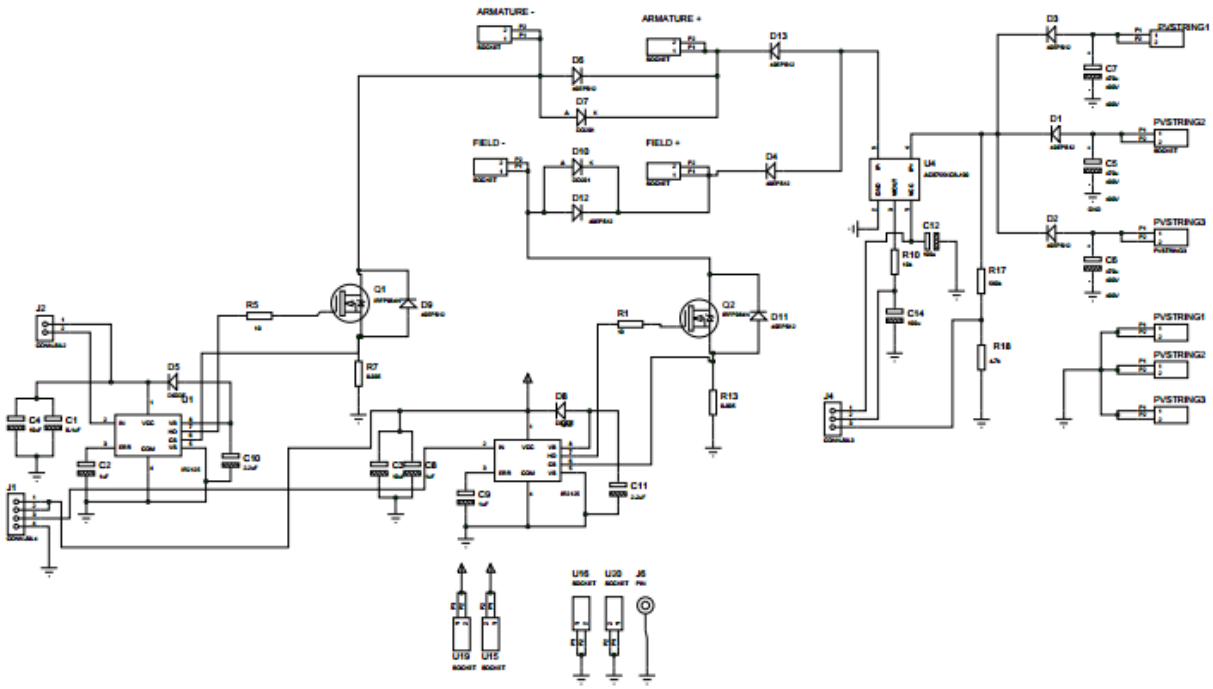

Figure 5.3 The MPPT circuit for the proposed photovoltaic water pumping system

B.5.4

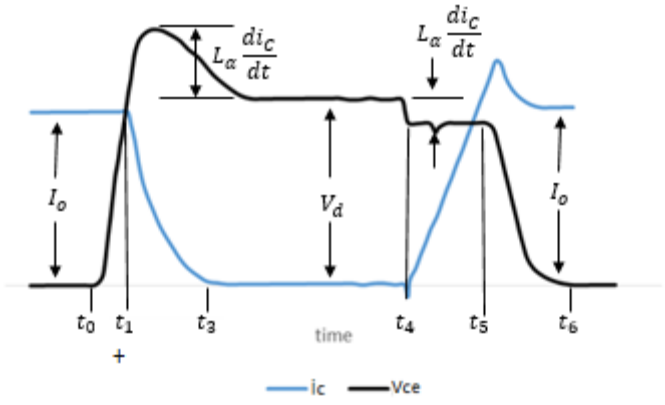

Figure 5.4 Current and voltage characteristics during turn on and turn off

B.5.5

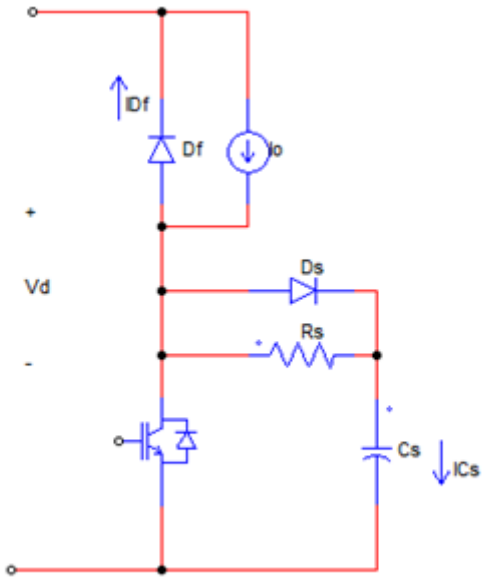

Figure 5.5 Turn off snubber circuit

B.5.6

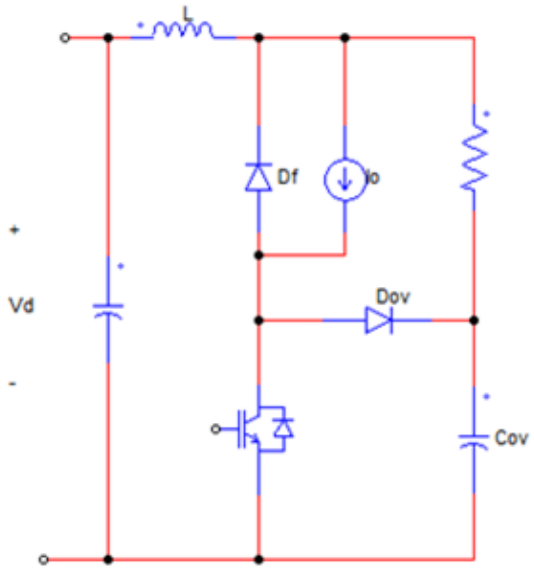

Figure 5.6 Overvoltage snubber circuit

B.5.7

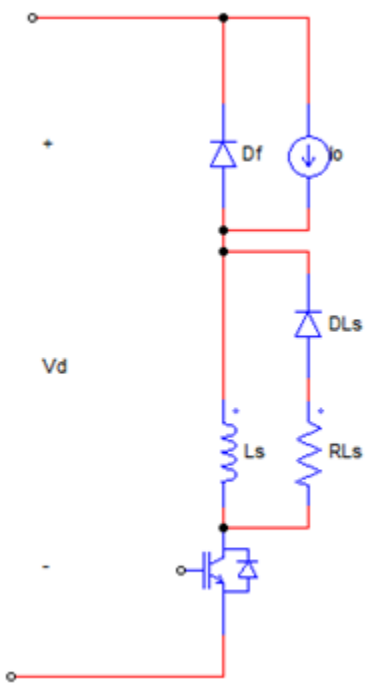

Figure 5.7 Turn on snubber circuit

Appendix C Tables

C.5.1

Table 5.1 Complex and absolute impedances of the DC motor at various frequency.

	Complex Impedance: $1.6 + J(f * 0.01319)\Omega$	Absolute Impedance
f=0Hz	1.6Ω	1.6Ω
f=100Hz	$1.6 + J1.3194\Omega$	2.07Ω
f=200H0z	$1.6 + J2.6389\Omega$	3.08Ω
f=400Hz	$1.6 + J5.2779\Omega$	5.51Ω
f=600Hz	$1.6 + J7.9168\Omega$	8.07Ω
f=800Hz	$1.6 + J10.555\Omega$	10.67Ω
f=1kHz	$1.6 + J13.194\Omega$	13.29Ω
f=2kHz	$1.6 + J26.389\Omega$	26.437Ω
f=4kHz	$1.6 + J52.778\Omega$	52.80Ω

C.5.2

Table 5.2 Separately excited DC motor data.

Rated Armature Voltage	220V
Armature Rated Voltage	220V
Armature Rated Current	23.5 A
Armature Resistance	2 ohm
Armature Inductance	6.153 mH
Field Rated Voltage	220 V
Field Rated Current	1.5 A
Field Resistance	76 ohm
Field Inductance	12.21 H
Rated Motor Speed	3000 rpm
Rated Motor Torque	15 N-m
Efficiency	88%

C.5.3

Table 5.3 Centrifugal pump data.

Power	5 HP
Flow Rate	42m3/h
Pressure Head	30m
Rated Speed	3000rpm

C.5.4

Table 5.4: KDM 230P PV module operating characteristics.

Maximum Power Voltage (Vmp)	30V
Maximum Power Current (Imp)	7.67A
Open Circuit Voltage (Voc)	36V
Short Circuit Current (Isc)	8.59A
Maximum Power at STC(Pmax)	230W
Module Efficieny	14.1%
Operating Module Temperature	-40℃ - +85℃,
Maximum System Voltage	DC 1000V
Maximum Series Fuse Rating	15A
Power Tolerance	+3/-0%
Mechanical Loading	5400Pa
STC: Irradiance 1000W/m^2, module temperature 25℃, AM=1.5;	

C.5.5

Table 5.5 Electrical characteristics of the PV module at various Solar irradiation.

Solar Irradiation (W/m^2)	200W/m^2,	400W/m^2,	600W/m^2,	800W/m^2,	1000W/m^2,
Maximum Power (Pmax)	36W	76W	120W	180W	230W
Maximum Power Voltage (Vmp)	23.17V	24.54V	25.95V	27.85V	30V
Maximum Power Current (Imp)	1.58A	3.10A	4.64A	6.45	7.67A

C.5.6

Table 5.6 Technical information of the IXXH50N60C3D1 IGBT.

Symbol	Test Conditions	Maximum Ratings
V_{CES}	$T_J = 25℃ \; to \; 175℃$	600V
V_{GES} V_{GEM}	Continuous Transient	$\pm 20V$ $\pm 30V$
$V_{CE(sat)} \leq 2.30V$	$I_C = 36A, V_{GE} = \pm 20V$	2.30V
I_{C25} I_{C110} I_{F110} I_{CM}	$T_C = 25℃$ $T_C = 110℃$ $T_C = 110℃$ $T_C = 25℃$, 1ms	100A 50A 30A 200A
$t_{d(on)}$ t_{ri} $t_{d(off)}$ t_{fi}	Inductive load, $T_J = 25℃$ $I_C = 36A$ $V_{GE} = 15V$ $V_{CE} = 360V$ $R_G = 5\Omega$	24ns 40ns 62ns 42ns
Q_g Q_{ge} Q_{gc}	$I_C = 36A, V_{GE} = 15V$ $V_{CE} = 0.5xV_{CES}$	$64nC$ $18nC$ $25nC$

C.5.7

Table 5.7 Power dissipation in the IGBT.

Frequency	$f = 200Hz$	$f = 400Hz$	$f = 800Hz$	$f = 1kHz$	$f = 2kHz$
IGBT: Power Dissipation	$36x10^{-3}\ W$	$72x10^{-3}\ W$	$145x10^{-3}\ W$	$180x10^{-3}\ W$	$360x10^{-3}\ W$

C.5.8

Table 5.8 Technical information of IR2125.

Symbol	Definition	Min.	Max.	Units
V_B	High Side Floating Supply Voltage	$V_S + 12$	$V_S + 12$	V
V_S	High Side Floating Supply Voltage	-5	500	V
V_{HO}	High Side Floating Supply Voltage	V_S	V_B	V
V_{CC}	Logic Supply Voltage	0	18	V
V_{IN}	Logic Input Voltage	0	V_{CC}	V
V_{ERR}	Error Signal Voltage	0	V_{CC}	V
V_{CS}	Current Sense Signal Voltage	V_S	V_B	V
T_A	Ambient Temperature	-40	125	℃
t_{on}	Turn on Propagation Delay	-	200	ns
t_{on}	Turn off Propagation Delay	-	190	ns
t_{on}	Turn on Rise Time	--	60	ns
t_{on}	Turn off Fall Time		35	ns

C.5.9

Table 5.9 Power dissipation in the gate driver.

Frequency	$f = 200Hz$	$f = 400Hz$	$f = 800Hz$	$f = 1kHz$	$f = 2kHz$
IGBT: Power Dissipation	$52x10^{-6}$	$104x10^{-6}$	$208x10^{-6}$	$260x10^{-6}$	$520x10^{-6}$

C.5.10

Table 5.10 Turn off snubber circuit design.

Symbol	Test Conditions	200W/m^2	1000W/m^2	Units
$W_R = \frac{C_s {V_d}^2}{2}$	Solar Irradiance: 200W/m^2-1000W/m^2	$8.5x10^{-6}$	$57.6x10^{-6}$	W
C_s		$0.5x10^{-9}$	$2x10^{-9}$	F
R_s		195	52	Ω

$t_{on\_state} >$	$f = 1Hz$	$0.224x10^{-6}$	$0.239x10^{-6}$	s

C.5.11

Table 5.11 Overvoltage snubber circuit design.

Symbol	Test Conditions	200W/m^2	1000W/m^2	Units
$W_C = \frac{C_{OV}\Delta V_{CE,max}{}^2}{2}$	Solar Irradiance: 200W/m^2 -1000W/m^2 Estimated Overvoltage =1V_d, $f = 1Hz$	$1.7x10^{-3}$	$11.5x10^{-3}$	W
kV_d		185	240	V
C_{ov}		$100x10^{-9}$	$400x10^{-9}$	F
L		195	52	H
$t_{on\_state} >$		$44.8x10^{-6}$	$47.8x10^{-6}$	s

C.5.12

Table 5.12 Turn on snubber circuit design.

Symbol	Test Conditions	200W/m^2	1000W/m^2	Units
$W = \frac{L_s I_o{}^2}{2}$	Solar Irradiance: 200W/m^2 -1000W/m^2 $\Delta V_{ce,max}$=150V, $f = 1Hz$	$0.14x10^{-6}$	$0.66x10^{-6}$	W
R_{Ls}		31.65	3.45	Ω
L		$1.26x10^{-6}$	$0.25x10^{-6}$	H
$t_{off\_state} >$		$91.56x10^{-9}$	$166.6x10^{-9}$	s

Appendix D Circuit Diagram

D.1.1

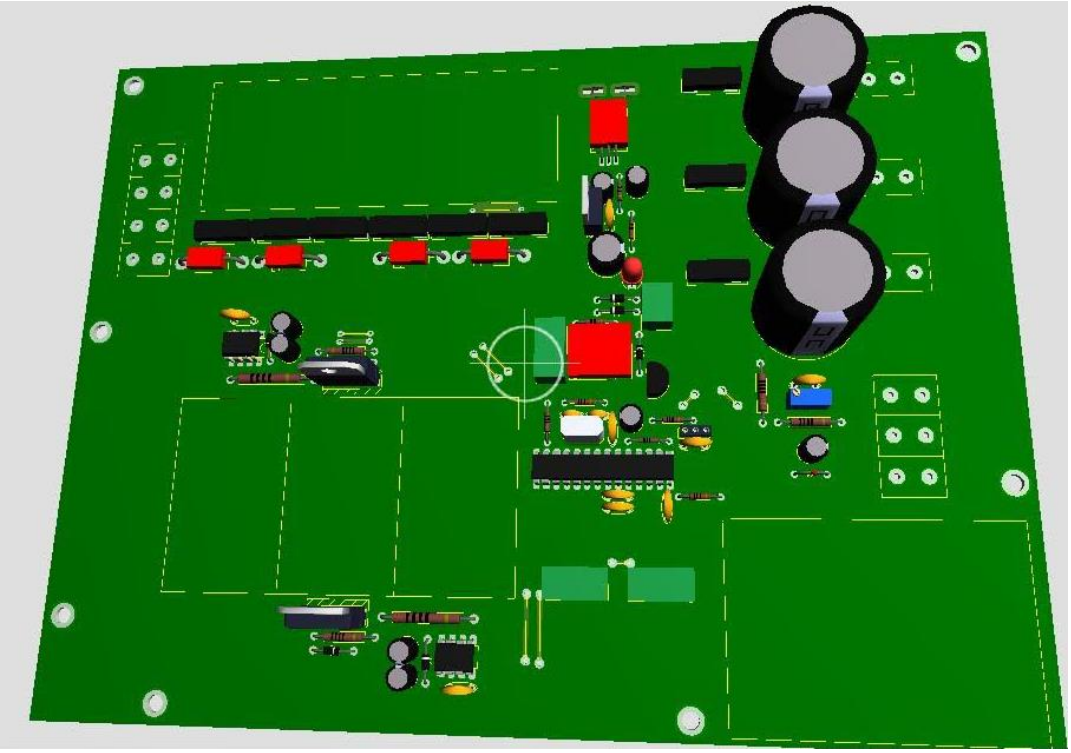

Diagram 1.1 The proposed MPPT circuit

D.1.2

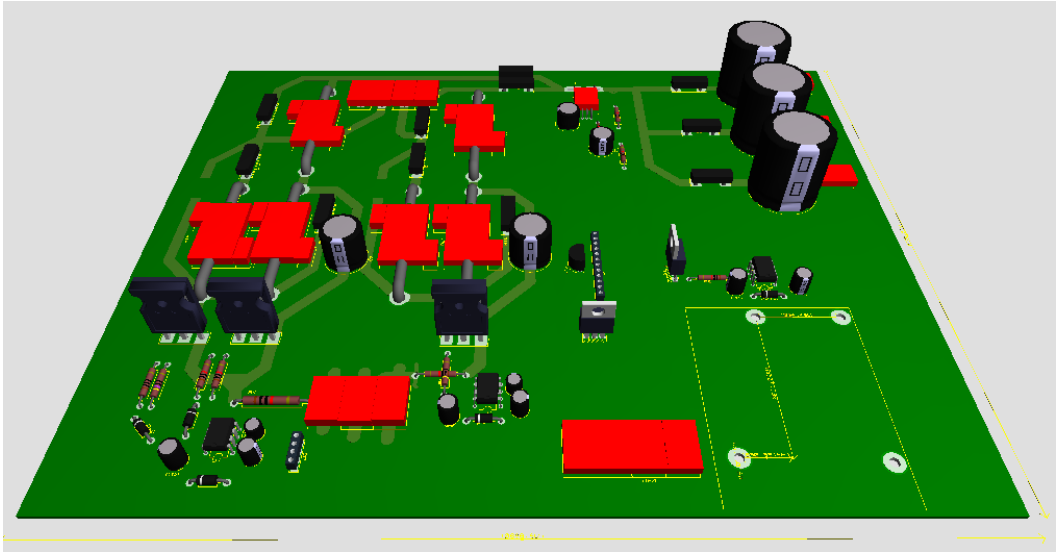

Diagram 1.2 The proposed MPPT circuit with snubber circuits

D.1.3

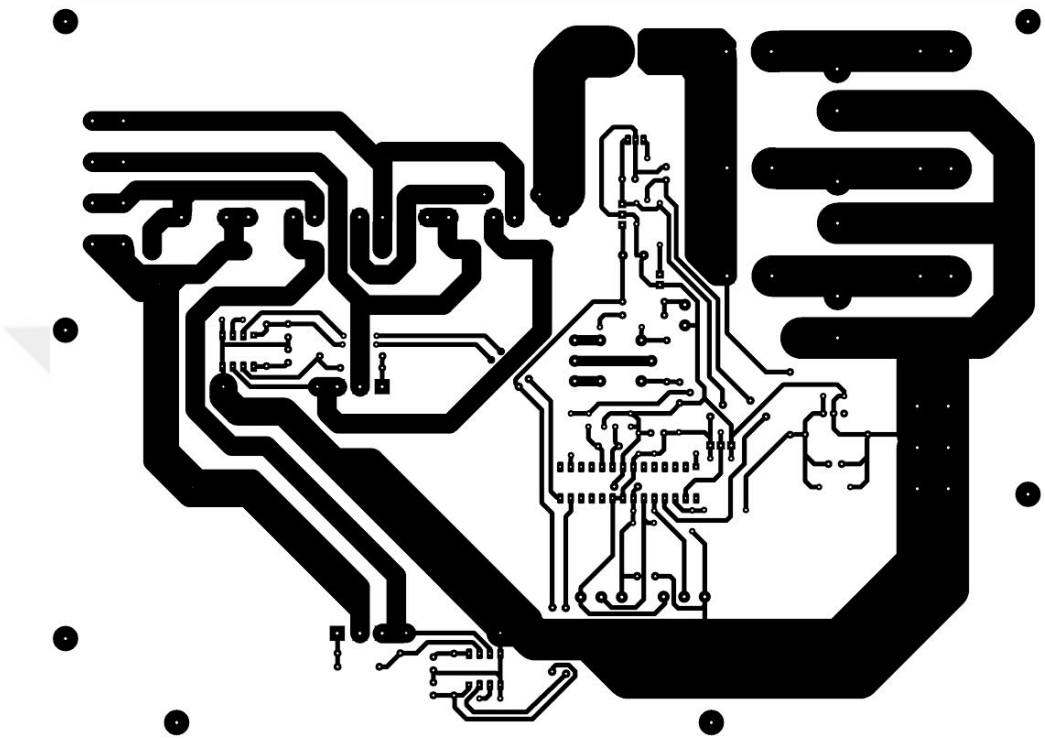

Diagram 1.3 Printed board diagram